Brain Structure and Function (2019) 224:1067–1095
https://doi.org/10.1007/s00429-018-01825-1

ORIGINAL ARTICLE

Cell-type specific parallel circuits in the bed nucleus of the stria terminalis and the central nucleus of the amygdala of the mouse

Jiahao Ye[1] · **Pierre Veinante**[1]

Received: 30 July 2018 / Accepted: 24 December 2018 / Published online: 4 January 2019

Abstract

The central extended amygdala (EAc) is a forebrain macrosystem which has been widely implicated in reward, fear, anxiety, and pain. Its two key structures, the lateral bed nucleus of the stria terminalis (BSTL) and the central nucleus of the amygdala (CeA), share similar mesoscale connectivity. However, it is not known whether they also share similar cell-specific neuronal circuits. We addressed this question using tract-tracing and immunofluorescence to reveal the EAc microcircuits involving two neuronal populations expressing either protein kinase C delta (PKCδ) or somatostatin (SOM). PKCδ and SOM are expressed predominantly in the dorsal BSTL (BSTLD) and in the lateral/capsular parts of CeA (CeL/C). We found that, in both BSTLD and CeL/C, PKCδ+ cells are the main recipient of extra-EAc inputs from the lateral parabrachial nucleus (LPB), while SOM+ cells constitute the main source of long-range projections to extra-EAc targets, including LPB and periaqueductal gray. PKCδ+ cells can also integrate inputs from the basolateral nucleus of the amygdala or insular cortex. Within EAc, PKCδ+, but not SOM+ neurons, serve as the major source of inputs to the ventral BSTL and to the medial part of CeA. However, both cell types can be involved in mutual connections between BSTLD and CeL/C. These results unveil the pivotal positions of PKCδ+ and SOM+ neurons in organizing parallel cell-specific neuronal circuits within CeA and BSTL, but also between them, which further reinforce the notion of EAc as a structural and functional macrosystem.

Keywords Central extended amygdala · Protein kinase C delta type · Somatostatin · Neuronal tracing · Microcircuit

Abbreviations

ac	Anterior commissure
ASt	Amygdalostriatal transition area
BDA	Biotin dextran amine, 10000 MW
BL	Basolateral nucleus of the amygdala
BLA	Basolateral nucleus of the amygdala, anterior
BLP	Basolateral nucleus of the amygdala, posterior
BMP	Basomedial nucleus of the amygdala, posterior
CARD	Combined catalyzed reporter deposition
CeA	Central nucleus of the amygdala
CeC	Central nucleus of the amygdala, capsular part
CeL	Central nucleus of the amygdala, lateral part
CeL/C	Central nucleus of the amygdala, lateral and capsular part
CeM	Central nucleus of the amygdala, medial part
CGRP	Calcitonin gene-related peptide
CGRPR	Calcitonin gene-related peptide receptor
CPu	Caudate putamen
CRF	Corticotropin-releasing factor
cst	Commissural stria terminalis
CTb	Cholera toxin B subunit
D2R	Dopamine receptor D2
DAPI	4′,6-Diamidino-2-Phenylindole, Dihydrochloride
DMPAG	Dorsomedial periaqueductal gray
DR	Dorsal raphe nucleus
EAc	Central extended amygdala
ENK	Enkephalin
FG	Fluorogold
Fu	Fusiform nucleus
GI/DI	Granular and dysgranular insular cortex
GP	Globus pallidus
Htr2a	Serotonin receptor 2a
i.p.	Intraperitoneal injection

✉ Jiahao Ye
yejiahao0@gmail.com

✉ Pierre Veinante
veinantep@inci-cnrs.unistra.fr

[1] Centre National de la Recherche Scientifique UPR3212, Institut des Neurosciences Cellulaires et Intégratives, Université de Strasbourg, 5 rue Blaise Pascal, 67000 Strasbourg, France

InsCx	Insular cortex
KLH	Keyhole limpet hemocyanin
LaVM	Lateral nucleus of the amygdala, ventromedial
LPAG	Lateral periaqueductal gray
LPB	Lateral parabrachial nucleus
LPBE	External lateral parabrachial nucleus
MPB	Medial parabrachial nucleus
NPY	Neuropeptide Y
PAG	Periaqueductal gray
PB	Phosphate buffer
PBS	Phosphate-buffered saline
PHA-L	*Phaseolus vulgaris* leucoagglutinin
Pir	Piriform cortex
PKCδ	Protein kinase C, delta type
Ppp1r1b	Phosphatase 1 regulatory subunit 1B
Rspo2	R-spondin 2
s.c.	Subcutaneous injection
S2	Secondary somatosensory cortex
scp	Superior cerebellar peduncle
SEM	Standard error of the mean
SOM	Somatostatin
BST	Bed nucleus of the stria terminalis
BSTL	Lateral bed nucleus of the stria terminalis
BSTLD	Dorsal lateral bed nucleus of the stria terminalis
BSTLP	Posterior lateral bed nucleus of the stria terminalis
BSTLV	Ventral lateral bed nucleus of the stria terminalis
BSTMA	Anterior medial bed nucleus of the stria terminalis
BSTMV	Ventral medial bed nucleus of the stria terminalis
VLPAG	Ventral lateral periaqueductal gray

Introduction

The central extended amygdala (EAc) is a forebrain macrosystem which contributes to diverse functions and disorders including fear and anxiety, stress reactions, emotional states, pain, reward learning, and addiction in animal models (Alheid 2003; de Olmos and Heimer 1999; Koob 2003; Lebow and Chen 2016; Neugebauer et al. 2004; Shackman and Fox 2016; Veinante et al. 2013; Waraczynski 2016). EAc is also increasingly gaining importance as a fundamental structure underlying psychiatric disorders such as anxiety disorders and posttraumatic stress disorder in human (Shackman and Fox 2016), but the structural organization of its neuronal microcircuits is still elusive.

The lateral part of the bed nucleus of the stria terminalis (BSTL) and the central nucleus of the amygdala (CeA) form the core structures of the EAc, and are anatomically continuous through cellular corridors along the stria terminalis, dorsally, and along the ventral amygdalofugal pathway, ventrally (Alheid 2003; Cassell et al. 1999). In the rodent brain, CeA has been divided into capsular (CeC), lateral (CeL), and medial divisions (CeM) (Cassell et al. 1999; Paxinos and Franklin 2012). In mice, however, the border between CeC and CeL is more elusive that in rats and diverse delineations have been applied in different studies (Haubensak et al. 2010; Kim et al. 2017; Li et al. 2013). Thus, we will refer to them collectively as capsular and lateral CeA (CeL/C). On the other hand, the delineation of BSTL subdivisions is less consensual (Alheid 2003; Dong et al. 2001a; Gungor and Pare 2016). In this study, we divided the middle BSTL level into dorsal (BSTLD), ventral (BSTLV), and posterior (BSTLP) parts, according to Paxinos and Franklin's mouse brain atlas (Paxinos and Franklin 2012). The BSTLD corresponds to the oval nucleus, which has been named as BSTov or BNSTov in the other studies (De Bundel et al. 2016; Dong et al. 2001b).

CeA and BSTL display striking similarities in cytoarchitecture, neurochemistry, and connectivity (Alheid 2003; Sun and Cassell 1993). The large majority of CeA and BSTL neurons are GABAergic, appearing morphologically similar to the medium-sized spiny neurons of the striatum, although a small number of glutamatergic neurons can be found in the BSTLV (Cassell et al. 1999; Kudo et al. 2012; Larriva-Sahd 2006; Nguyen et al. 2016; Sun and Cassell 1993). EAc GABAergic neurons give rise to local intra-nuclear inhibitions (Cassell et al. 1999; Hunt et al. 2017; Sun and Cassell 1993), mutual inhibitions between BSTL and CeA (Sun and Cassell 1993; Sun et al. 1991; Veinante and Freund-Mercier 1998), and long-range inhibitory projections (Moga et al. 1989; Sun and Cassell 1993). These EAc GABAergic projection neurons can express different neuropeptides, such as somatostatin (SOM), corticotrophin-releasing factor (CRF), and neurotensin (NT), but not enkephalin (ENK) (Gray and Magnuson 1987, 1992; Hopkins and Holstege 1978; Veening et al. 1984). At mesoscopic level, both BSTL and CeA are targeted by similar cortical, intra-amygdaloid, thalamic, and brainstem afferents, and both project to the same hypothalamic and brainstem targets (Alheid 2003; Davis and Shi 1999; McDonald et al. 1999). In addition, BSTL and CeA are strongly linked by subdivision-specific interconnections, and a directional bias in intrinsic EAc connections has been suggested from BSTLD and CeL/C to ventral BSTL (BSTLV) and to CeM (Cassell et al. 1999; Sun et al. 1991).

Recent studies revealed the existence of two non-overlapping neuronal groups in the mouse CeL/C, expressing either protein kinase C delta type (PKCδ) or somatostatin (SOM) and together constituting the majority of local GABAergic neurons (Haubensak et al. 2010; Li et al. 2013). PKCδ+ and SOM+ neurons can form local disinhibitory circuits controlling fear learning (Ciocchi et al. 2010; Fadok et al.

2017; Haubensak et al. 2010; Li et al. 2013), sustained anxiety (Botta et al. 2015), active defense (Yu et al. 2016), and feeding behavior (Cai et al. 2014; Campos et al. 2016). Yet, it is unknown whether BSTL shares some features of cell-type specific circuits with CeA. On one hand, the BSTL is similarly enriched with mRNA expressing PKCδ and SOM as the CeA is (Lein and et al. 2007). On the other hand, BSTL is also involved in fear responses and anxiety-related behaviors, even though CeA and BSTL could have distinct roles (Davis et al. 2010; De Bundel et al. 2016; Jennings et al. 2013; Kim et al. 2013; Mazzone et al. 2016). Based on the idea that components of EAc are similarly organized, we further hypothesize that, similar to CeA, microcircuits based on PKCδ+ or SOM+ neurons might also exist in the BSTL, which contributes to intra- and extra-EAc circuits.

In this study, we combined tract-tracing and immunofluorescence in mice to dissect the neuronal microcircuits of BSTL and CeA at three levels: long-range inputs, intrinsic EAc connectivity, and long-range outputs. Our results show that both PKCδ+ and SOM+ neuronal populations are similarly involved in microcircuits of CeL/C and BSTLD. In both CeL/C and BSTLD, PKCδ+ neurons are preferentially innervated by calcitonin gene-related peptide (CGRP)-positive inputs from the lateral of the parabrachial nucleus (LPB), especially its external part (LPBE), and can also integrate the other long-range excitatory inputs, from insular cortex (InsCx) and posterior basolateral nucleus of the amygdala (BLP). The PKCδ+ population also provides the main inhibition within EAc, via projections to CeM and BSTLV. On the other hand, mutual connections between BSTLD and CeL/C can be mediated by both cell types. In comparison, SOM+ neurons contribute to the main outputs from BSTLD and CeL/C to extra-EAc targets, including LPBE and periaqueductal gray (PAG).

Materials and methods

Animals

Adult male C57BL/6J mice of 11–12 weeks old (Charles River®, L'Arbresle, France) were housed in standard housing cages, with ad libitum access to food and water (12/12-h light/dark cycle). In total, 27 mice were used for this study. All the experimental procedures were carried out in accordance with the regulations from European Communities Council Directive and approved by the local ethical committee (CREMEAS under reference AL/61/68/02/13).

Stereotaxic tract-tracing

Individual animal was anesthetized by an intraperitoneal injection (i.p.) of a mixture of ketamine (87 mg/kg) and xylazine solution (13 mg/kg). Then, the deep-anesthetized animal was treated with metacam (2 mg/kg, subcutaneous, or s.c.) to alleviate inflammatory response and bupivacaine (2 mg/kg, s.c.) was infiltrated on the scalp to induce local analgesia. After that, the mouse was mounted into a stereotaxic frame (Model 900, David Kopf Instrument) and a small craniotomy was made with surgical drill allowing for passage of glass pipette.

Solution of tracers were loaded into a glass pipette (tip diameter 15–25 µm) that was pulled with a P-97 micropipette puller (Sutter Instrument) and positioned according to the stereotaxic coordinates (Paxinos and Franklin 2012) (Table 1). The tracers were injected either by iontophoresis with a constant current source (Midgard Model 51595, Stoelting Co.) or by pressure injection (Picospritzer® III, Parker Hannifin Corp). Two different tracers were used for anterograde tracing. Biotin dextran amine, 10,000 MW (BDA; 2% or 4% in phosphate buffer saline, PBS; cat. #D1956, Molecular Probe®) or *Phaseolus vulgaris* leucoagglutinin (PHA-L; 2.5% in phosphate buffer, PB; cat. #L-1110, Vector Laboratories®) was injected for 10–15 min (+3–5 µA, 7 s ON/OFF cycle). Three different tracers were used for retrograde tracing. First, hydroxystilbamidine methanesulfonate (cat. #A22850, Molecular Probes®) or aminostilbamidine (cat. #FP-T8135A, Interchim®) (indicated together as Fluorogold, or FG; 2% in 0.9% NaCl) was injected for 10 min (+2 µA, 3 s ON/OFF cycle). Second, cholera toxin B subunit (CTb; 0.25% in 0.1 M Tris buffer and 0.1% NaCl; cat. #C9903, Sigma®) was injected for 15 min (+4–5 µA, 3 s ON/OFF cycle). The third tracer, red Retrobeads™ (50–150 nL; Lumafluor Inc.), was injected into regions of interest with a Picrospritzer® III.

After the injection, the pipette was kept in place for 5–10 min before withdrawing. The scalp was then closed

Table 1 Stereotaxic coordinates of tracers injections

Brain areas	Coordinates		
	AP (mm)	ML (mm)	DV (mm)
BSTLD	+0.20	+0.90	− 3.30
BSTLV	+0.20	+0.90	− 4.00
CeL/C	− 1.43	+2.35	− 3.75
CeM	− 1.07	+2.20	− 4.00
LH	− 1.55	+1.00	− 4.60
vlPAG	− 4.47	+0.40	− 2.70
LPBE	− 5.19	+1.60	− 3.60

The stereotaxic coordinates are taken from Paxinos and Franklin's mouse brain atlas (Paxinos and Franklin 2012), with the bregma point as the origin for AP and ML axis. The DV distance was referred to its cortical surface at the corresponding AP, ML location

AP Antero-posterior axis, *ML* Medial–Lateral axis, *DV* dorsal–ventral axis

and a lidocaine spray (2%, Xylovet®) was infiltrated near the wound. The animal was monitored by the experimenter until waking up and was placed in his home cage in the animal facility for 7–14 days to allow the transport of the tracers.

Sections preparation

The animal was killed by a lethal dose of pentobarbital (273 mg/kg, i.p.) or Dolethal (300 mg/kg, i.p.). After checking the disappearance of toe-pinch reflex, the animal was transcardially perfused with ice-cold phosphate buffer for 1 min (PB; 0.1 M, pH 7.4; 10 mL) and then with fixative (2% paraformaldehyde, in 0.1 M PB, pH 7.4; 150 mL) for 15 min. The brain was removed and placed overnight for post-fixation in the fixative (4 °C). Then, brains were kept in phosphate-buffered saline (PBS, Cat. # ET300-A, Euromedex, France; 4 °C) for 1 week or in PBS-sodium azide (0.02%) for longer time before sectioning. Serial coronal sections (thickness 30 µm) were cut with a vibratome (VT1000S, Leica Biosystem). Sections were kept in PBS (4 °C) for use within 1 week or in sodium azide (0.02% in PBS) for longer time. Subsequent immuno- and histo-fluorescence procedures were then carried out on selected brain sections (120 µm apart for adjacent slices) for each animal. The procedures were carried out to simultaneously visualize PKCδ+ and/or SOM+ neurons together with the tracers and/or another cellular marker of interest (i.e. CGRP), through different combinations of primary and secondary antibodies.

Combined catalyzed reporter deposition (CARD) for somatostatin

In our hands, a traditional immunofluorescence staining of SOM revealed only a few cell bodies in BSTLD and CeL/C, probably due to the low content of neuropeptide in the soma of projection neurons. To get robust staining of SOM+ cell bodies in EAc, we, thus, applied a highly sensitive method known as the combined catalyzed reporter deposition (CARD) (Hunyady et al. 1996; Speel et al. 1997). With the catalytic power of horseradish peroxidase, the CARD method allows specific deposits of tyramide conjugates nearby the antigen. The reaction can amplify the immunochemical signal up to a 10–100-fold, compared to that of general immunofluorescence staining (Hunyady et al. 1996). In this study, we use fluorochrome-conjugated tyramide (i.e., fluorescein tyramide and Cy3 tyramide) to reveal SOM signal. All procedures were carried out in floating brain sections, at room temperature, unless specified otherwise. First, the intrinsic peroxidase activity of brain slices was inhibited by 1% H_2O_2 in 50% ethanol solution for 20 min. Sections were then washed with PBS (3 × 5 min) and blocked with the blocking buffer (Triton X-100 0.3% and donkey serum 5% in PBS) for 45 min. After that, sections were incubated overnight with rabbit-anti-somatostatin antibodies (Table 2) in dilution buffer (Triton X-100 0.3% and donkey serum 3% in PBS). Then, the sections were washed with PBS (3 × 5 min) and incubated with the HRP-conjugated donkey anti-rabbit antibody (1:300, in dilution buffer) for 3 h. Sections were then washed in PBS (2 × 5 min) and then in PBS-imidazole buffer (100 mM, pH 7.6; 5 min). Finally, the CARD reaction was carried out with fluorescein tyramide or Cy3 tyramide (1:1000, a gift from Prof. Klosen, University of Strasbourg) in PBS–imidazole buffer and H_2O_2 (0.001%) for up to 30 min. The reaction was stopped by washing off with PBS (3 × 5 min). The same CARD procedures were also used to reveal BDA-labeled axons (i.e. Figs. 4, 5) when the signal was weak with the traditional histo-fluorescence staining. In those cases, peroxidase was introduced by incubation of ABC-HRP system (1:500; Cat. # PK-6100, Vector Laboratories™) for 1.5 h (room temperature).

Immunofluorescence staining

General immunofluorescence staining of other antigens was carried out after CARD revelation of SOM, when applicable. Thus, SOM immunoreactivities, together with a tracer

Table 2 Primary antibodies

Name	Species, poly/mono-	Dilution	Antigen	Source, catalog etc.	References
CGRP	Rabbit, polyclonal	1:1500	Rat CGRP	Cat. #RPN1842, Amersham	Franke-Radowiecka (2011)
CTb	Goat, antiserum	1:3000	choleragenoid	Cat. #703, List Biological Laboratories	Thompson and Swanson (2010)
FG	Rabbit, polyclonal	1:1000	KLH-conjugated Fluorescent Gold	Cat. #AB153-I, Millipore	Thompson and Swanson (2010)
PHA-L	Goat, polyclonal	1:1000	pure lectin	Cat. #AS-2224, Vector Laboratories	Thompson and Swanson (2010)
PKCδ	Mouse, monoclonal	1:1000	Human PKCδ aa. 114–289	Cat. #610398, BD Biosciences	Haubensack et al. (2010)
SOM	Rabbit, antiserum	1:5000	KLH-conjugated synthetic somatostatin (AGCKNFFWKTFTSC)	Cat. #20067, Immunostar	Jhou et al. (2009)

(i.e., CTb or FG) or other cellular markers of interest (i.e., PKCδ or CGRP), were simultaneously visualized with the combinations of different primary antibodies (see Table 2) and secondary antibodies, following the general procedure described below. After finishing the CARD revelation of SOM, a combination of primary antibodies was applied overnight at room temperature in dilution buffer. The combination depended on the aim of each experiment, type of tracers, and technical constraints. For example, we added PKCδ primary antibodies to show the spatial distribution of PKCδ+ and SOM+ neurons, but also used PKCδ and CGRP immunofluorescence to analyze the apposition of CGRP terminals onto labeled neurons in EAc.

Sections were then washed in PBS (3 × 5 min) and incubated with corresponding secondary antibodies (1:300 in dilution buffer) for 3 h at room temperature. Diverse fluorophore-conjugated secondary antibodies were chosen for triple labeling of SOM, PKCδ, and the third antigen, based on the compatibility of fluorophores. Overall, the following secondary antibodies were used: donkey anti-mouse-Alexa-647 conjugates (Cat. #: A-31571, Invitrogen™), donkey anti-mouse-Cy3 conjugates (Cat. #: 715-165-151, Jackson Immunoresearch™), donkey anti-rabbit-Cy5 (Cat. #: 711-175-152, Jackson Immunoresearch™), donkey anti-rabbit-Alexa 488 (Cat. #: A-21206, Invitrogen™), donkey anti-goat-Alexa 488 (Cat. #: A-11055, Invitrogen™). Streptavidin-Alexa 488 conjugate (1: 750; Cat. #: S32354, Molecular Probe®) was used for the visualization of BDA.

After washing in PBS (3 × 5 min), the sections were counterstained with DAPI (4′,6-diamidino-2-phenylindole, dihydrochloride; 300 nM, Cat. # D1306, Invitrogen™) for 3–5 min. The sections were then arranged onto Superfrost® plus slides (Thermo Fisher Scientific™) and mounted in Fluoromount™ medium (Cat. #: F4680, Sigma-Aldrich™).

The use of CARD revelation made it possible to stain two different of antigens with two different primary antibodies from the same species (Hunyady et al. 1996). In this study, we used different rabbit antibodies for SOM, FG, and CGRP. For instance, to simultaneously visualize PKCδ, SOM, and CGRP, a low concentration of rabbit-anti-SOM (1:5000) was used for CARD revelation, and a higher concentration of rabbit-anti-CGRP (1:1000) antibody was subsequently applied. In this way, SOM and FG or CGRP could be revealed with the sequential applications of primary antibodies from rabbit, without showing detectable cross-staining. The absence of cross-staining was determined by the separation of the staining patterns and by negative control experiments in which CGRP primary antibodies were omitted.

Imaging and analysis

For each animal, the location of injection core of tracer was examined on successive sections containing the injection sites and was evaluated according to salient anatomical (i.e., fiber bundles) and neurochemical features (i.e., DAPI staining and PKCδ immunoreactivity). The delineation of subdivisions of EAc, LPB, PAG, InsCx, and BLP was done according to the fourth edition of mouse brain atlas (Paxinos and Franklin 2012). Cases in which the injection sites spilled beyond the target in nearby regions were not included into the data analysis.

For illustrations of injection sites and neurochemical patterns, if not stated otherwise, epifluorescence images were acquired by an Axio Imager 2 (Carl Zeiss™) microscope equipped with a digital camera (ProgRes® CFcool, Jenoptik, GmbH, Germany), under 10x, or 20x objectives; or by a NanoZoomer S60 (Hamamatsu Photonics) under a 20x objective.

To demonstrate the co-localization of markers and potential appositions between neurons and axonal processes, confocal imaging at the middle focal plane of the section was taken with a Leica TCS SP5 II system (Leica Biosystem). Images were sampled to a pixel resolution of 0.255 µm by 2.5-fold of Nyquist sampling, under 20x objective with 1 airy unit. To gain more details of axonal apposition, single plane or z-stack (1 µm) confocal images were taken under 63x objective.

For quantitative analysis of co-localization, epifluorescence images were taken with Axio Imager 2, under 20x apochromatic objectives. A z-stack image (step size = 2.049 µm) was obtained in BSTLD (bregma + 0.13 mm) or CeA (bregma − 1.43 mm) for each animal. The co-localization of tracers with PKCδ+ or SOM+ neurons in epifluorescence was also confirmed by corresponding confocal images. Preprocessing of images, primarily for pseudo-coloring and adjusting contrast, and subsequent analysis including cell counting and co-localization were carried out manually on open software FIJI (Schindelin et al. 2012).

Statistics

For co-localization and apposition studies, mean value and standard error of the mean (SEM) are reported by injection group and brain areas. Unpaired two-sample Student's *t* test was carried out in R program (©The R Foundation).

Results

Distribution of PKCδ neurons and SOM neurons in BSTLD and CeL/C

We first examined the pattern of PKCδ and SOM immunoreactivities in subdivisions of the BSTL ($n = 3$) and of the CeA ($n = 3$). PKCδ+ soma were detected mainly

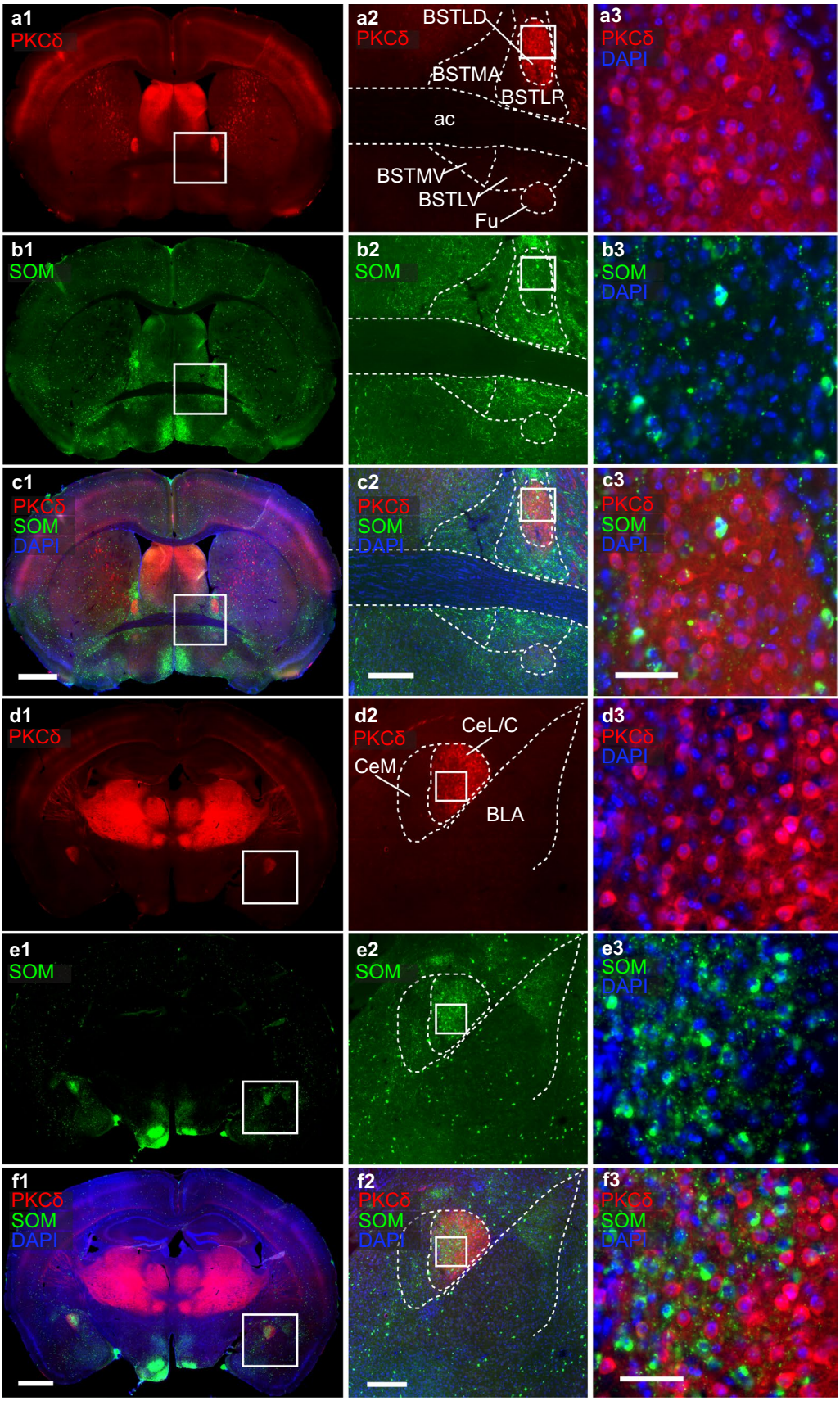
a1
PKCδ
a2
PKCδ
BSTLD
BSTMA
BSTLR
ac
BSTMV
BSTLV
Fu
a3
PKCδ
DAPI
b1
SOM
b2
SOM
b3
SOM
DAPI
c1
PKCδ
SOM
DAPI
c2
PKCδ
SOM
DAPI
c3
PKCδ
SOM
DAPI
d1
PKCδ
d2
PKCδ
CeL/C
CeM
BLA
d3
PKCδ
DAPI
e1
SOM
e2
SOM
e3
SOM
DAPI
f1
PKCδ
SOM
DAPI
f2
PKCδ
SOM
DAPI
f3
PKCδ
SOM
DAPI

◂**Fig. 1** PKCδ- and SOM-expressing cells are concentrated in BSTLD and CeL/C. Double staining of PKCδ (**a, c, d, f**; red) and SOM (**b, c, e, f**; green) in coronal sections of BSTLD (**a–c**; bregma level + 0.13 mm) and CeL/C (**d–f**; bregma − 1.55 mm), detected with epifluorescence. DAPI staining (blue) of cell nuclei is also shown (c1, f1, c2, f2 and a3–f3). The first column shows a view of full sections at the level of the BSTL (a1–c1) and of the amygdala (d1–f1); the second column shows a detailed view of BSTL (a2–c2) and amygdala (d2–f2) with delineations, corresponding to the boxed area in a1–f1; the third column shows a magnification at cellular level in the BSTLD (a3–c3) and in the CeL/C (d3–f3) of the boxed areas in a2–f2. See list for abbreviations. Scale bars: a1–f1, 1.0 mm; a2–f2, 500 µm; a3–f3, 50 µm

in the BSTL and CeA, as well as in the lateral septum (Fig. 1a) and the thalamus (Fig. 1d). In BSTL, well-stained PKCδ+ cell bodies were concentrated in the BSTLD, of which they highlighted the oval shape, with sharp contrast compared to the absence of labeling in the surrounding BSTLP (Fig. 1a). In CeA, PKCδ+ soma were present in CeL/C where they tended to be concentrated laterally, with a reduced density medially, at the limit with the CeM (Fig. 1d). Densely packed PKCδ+ neuropil was also obvious in BSTLD and CeL/C (Fig. 1a, d; see also Fig. 2c, e, f). SOM+ neurons were observed mainly in the BSTL, cerebral cortex, caudate putamen, hypothalamus (Fig. 1b), and amygdala (Fig. 1e). While the staining of SOM+ interneurons in cerebral cortex and caudate putamen filled the cell bodies, the SOM labeling of somas in BSTL and CeA was patchier and hardly defined the somatic contours, probably due to the low content of SOM in the soma of projection neurons. In the BSTL, SOM+ neurons and fibers were observed in all subdivisions, including BSTLD (Fig. 1b, see also Fig. 2b), where their distribution overlapped with that of PKCδ+ neurons (Fig. 1c). In the CeA, a low density of SOM+ somas and processes appeared in the CeM, but a strong concentration was observed in the CeL/C (Fig. 1e). The distribution of SOM+ cell bodies overlapped with that of PKCδ+ neurons medially (i.e., CeL), but decreased laterally (i.e., CeC), where PKCδ+ neurons were the most abundant (Fig. 1f). Despite their similar regional distribution in BSTLD and CeL/C, PKCδ and SOM immunoreactivities remained segregated at cellular level and were almost never observed in the same neurons (Fig. 1c, f; see also Fig. 2c, e). Finally, while PKCδ+ and SOM+ neurons were observed along the rostrocaudal extent of BSTLD (bregma + 0.25 mm to + 0.01 mm) and CeL/C (bregma − 0.80 mm to − 2.03 mm), their density appeared stronger in the caudal parts of BSTLD and CeL/C.

Thus, we confirmed the expression of the similar cellular markers, PKCδ and SOM, in segregated neuronal populations of CeL/C, in accordance with the previous descriptions (Ciocchi et al. 2010; Haubensak et al. 2010; Li et al. 2013), and showed that a similar situation occurs in BSTLD.

A majority of PKCδ+ neurons are closely surrounded by CGRP+ terminals

Having established the distribution of PKCδ+ and SOM+ neurons in BSTLD and CeL/C, we tested whether external inputs could target similar populations in both nuclei. The LPB is known to provide a dense input to BSTLD and CeL/C (Alden et al. 1994; Bernard et al. 1993). This LPB–EAc pathway is characterized by large basket-like pericellular terminals (Sarhan et al. 2005) co-releasing glutamate and neuropeptides, especially CGRP (Delaney et al. 2007; Salio et al. 2007). As the CGRP innervation to EAc has been shown to originate essentially from LPB in rats (D'Hanis et al. 2007; Yasui et al. 1991b), and as a recent study in mice suggested that the cells expressing CGRP receptor overlap with SOM and PKCδ populations (Han et al. 2015), we first examined the potential innervation of SOM and PKCδ by CGRP terminals using a triple immunofluorescence protocol (Fig. 2).

In accordance with the previous descriptions, CGRP+ terminals were observed in the BSTLD and the CeL/C. Their distribution largely overlapped with that of PKCδ+ cells and partially overlapped with that of SOM+ cells (Fig. 2b, d) and displayed characteristic perisomatic terminals (Fig. 2c, e). Confocal analysis at cellular level showed that PKCδ+ somas were often surrounded by basket-like CGRP+ elements in BSTLD (Fig. 2c) and CeL/C (Fig. 2e). A close observation revealed the wrapping of soma and proximal dendrites of PKCδ+ neurons by CGRP+ terminals (Fig. 2f). A quantitative analysis ($n = 3$) indicated that 84.4% and 80.6% of PKCδ+ soma in BSTLD and CeL/C, respectively, were closely surrounded by CGRP+ perisomatic terminals (Fig. 2a). In addition, most of CGRP+ baskets-like structures contact either PKCδ+ neurons or PKCδ-negative/SOM-negative (PKCδ−/SOM−) neurons.

By contrast, CGRP+ basket-like structures almost never surrounded SOM+ somas in BSTLD (Fig. 2c) or CeL/C (Fig. 2e, f). Yet, we cannot exclude that thinner single CGRP+ terminal lacking the basket-like appearance, could contact SOM+ neurons, as such putative appositions were sometimes registered under high magnification (Fig. 2f). However, the incomplete staining of SOM+ soma did not allow validating the existence of such contacts.

Thus, these evidences support a dominant perisomatic CGRP+ innervation onto PKCδ+, but not SOM+, neurons in EAc, even though an underestimated number of SOM+ neurons in BSTLD and CeL/C were labeled in our study. In addition, non-perisomatic contacts between CGRP+ terminals and SOM+ neurons can not be excluded.

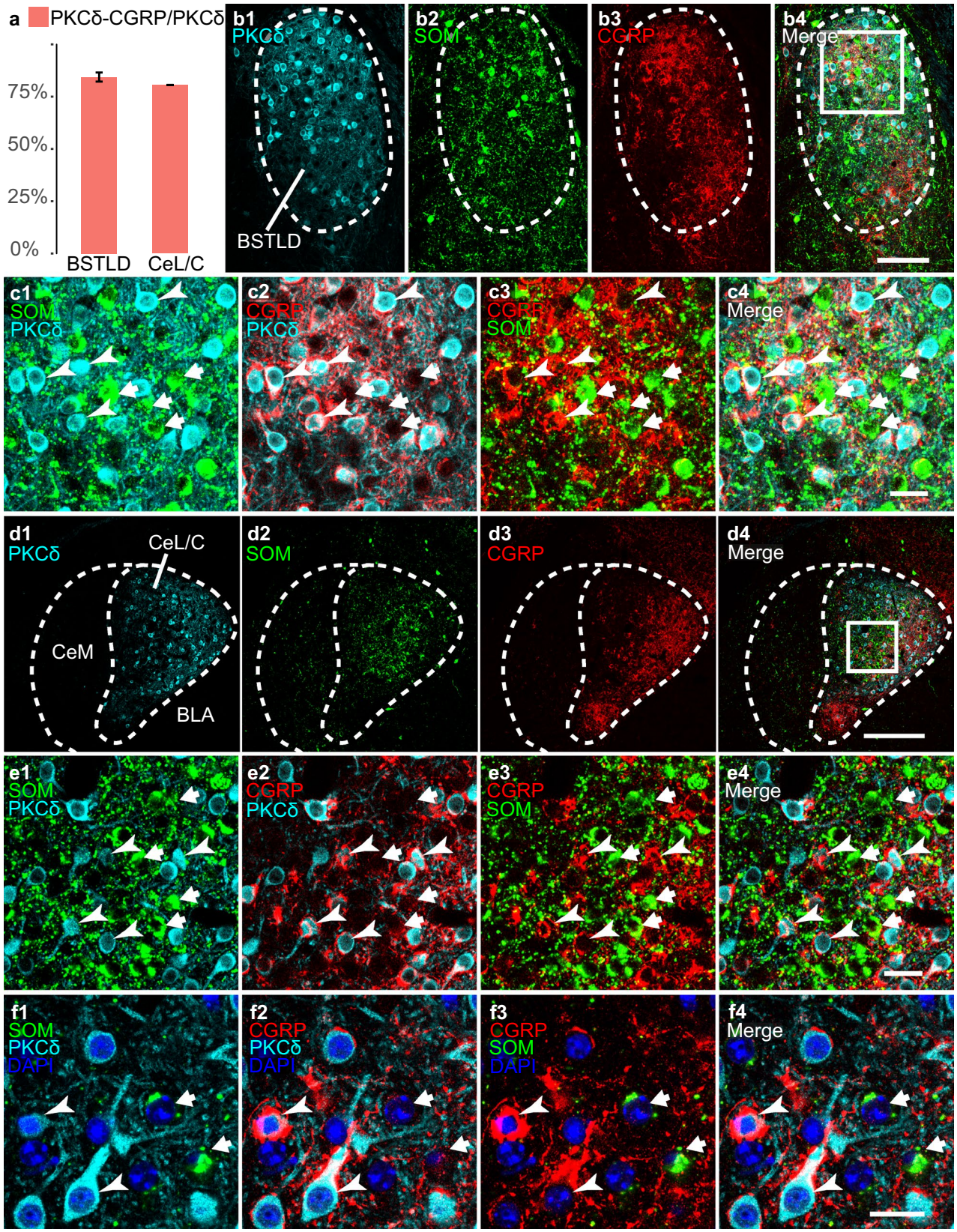
a
PKCδ-CGRP/PKCδ
75%
50%
25%
0%
BSTLD
CeL/C
b1
PKCδ
BSTLD
b2
SOM
b3
CGRP
b4
Merge
c1
SOM
PKCδ
c2
CGRP
PKCδ
c3
CGRP
SOM
c4
Merge
d1
PKCδ
CeL/C
CeM
BLA
d2
SOM
d3
CGRP
d4
Merge
e1
SOM
PKCδ
e2
CGRP
PKCδ
e3
CGRP
SOM
e4
Merge
f1
SOM
PKCδ
DAPI
f2
CGRP
PKCδ
DAPI
f3
CGRP
SOM
DAPI
f4
Merge

◂**Fig. 2** Structural apposition of CGRP+ terminals onto PKCδ+ neurons in BSTLD and CeL/C. Confocal imaging of triple labeling for PKCδ (cyan), SOM (green) and CGRP (red) in BSTLD (**b, c**) and CeL/C (**d–f**). **a** Percentages of PKCδ+ somas in putative contact with perisomatic CGRP+ terminals, for BSTLD (Mean = 84.4%, SEM = 0.031, n = 3) and CeL/C (Mean = 80.6%, SEM = 0.0005, n = 3). b1–b4, d1–d4: Low-power view of BSTLD (b1–b4) and CeL/C (d1–d4) showing the distribution of PKCδ (b1, d1), SOM (b2, d2),CGRP (b3, d3) immunoreactivities and the three signals merged (b4, d4). c1–c4, e1–e4: Magnifications at cellular level of the boxed areas in b4 (BSTLD) and d4 (CeL/C) showing signals for PKCδ and SOM (c1, e1), CGRP and PKCδ (c2, e2), CGRP and SOM (c3, e3), and merge (c4, e4); the arrows point to PKCδ+ neurons and the arrowheads point to SOM+ neurons (same in f1–f4). Note the absence of overlap between PKCδ+ and SOM+ somas (c.1, e.1), the frequent appositions of CGRP+ baskets around PKCδ+ somas (c2, e2), and the absence of such appositions onto SOM+ somas (c3, e3). In f1–f4, a further magnification in BSTLD leads to the same observations and shows that CGRP+ baskets wrapped around soma and primary dendrites of PKCδ+ somas. See the list. Scale bars: b.1–b4, 100 µm; c1–c4, 25 µm; d1–d4, 200 µm; e1–e4, 25 µm; f1–f4, 20 µm

CGRP terminals from LPB target PKCδ neurons in EAc

To further confirm the possibility that CGRP+ axonal terminals contacting EAc PKCδ+ neurons were derived from the LPB, we performed BDA anterograde tracing from LPB, followed by subsequent triple fluorescent labeling.

BDA injection sites in LPB ($n = 5$) were centered in the LPBE (mainly from bregma − 5.07 mm to − 5.41 mm), with occasional expansion into neighboring central lateral and dorsal subnuclei (LPBcl, LPBd), but never extending to medial parabrachial nucleus or Kölliker–Fuse nucleus (Fig. 3a, f). In the ipsilateral EAc, BDA+ axons were primarily located in the BSTLD (Fig. 3b, g), fusiform nucleus of ventral BSTL (not shown), and CeL/C (Fig. 3d, i), with only a few axonal processes in BSTLP or CeM. At higher magnification, distinct BDA+ perisomatic arrangements were observed, along with individual fibers (Fig. 3c, e, h, j). The comparison of BDA+ and CGRP+ signals showed that a substantial number of the BDA+ axons, forming basket-like structures, also contained CGRP signal. Conversely, CGRP+ basket-like structures were often coincident with BDA+ labeling (Fig. 3c, e, h, j). However, some CGRP+ perisomatic formations appeared to be BDA−, and individual BDA+ axons only partially overlapped with CGRP immunoreactivity.

Triple labeling for PKCδ, CGRP, and BDA (Fig. 3a–e) showed that the large majority of the PKCδ+ somas in BSTLD (Fig. 3c) and CeL/C (Fig. 3e) were surrounded by CGRP+ baskets, as shown in the previous experiment, including most of the BDA+/CGRP+ baskets. In addition, a number of BDA+/CGRP− axonal segments were also found in close apposition with PKCδ+ somas. In sections processed for triple labeling for SOM, CGRP, and BDA (Fig. 3f–j), basket-like terminals revealed by BDA and/or CGRP signals very rarely contacted SOM+ cell bodies, albeit simple BDA+/CGRP− terminals could be found in close proximity to SOM+ somas in BSTLD (Fig. 3h) and CeL/C (Fig. 3j).

Thus, the preferential perisomatic CGRP innervation onto PKCδ+, but not SOM+, neurons in BSTLD and CeL/C, is likely to derive, at least in part, from the LPBE. In addition, the observation of BDA+/CGRP− perisomatic terminals surrounding PKCδ+ neurons and of individual axons found close to PKCδ+ or SOM+, suggest the existence of CGRP and non-CGRP inputs from LPBE to EAc.

PKCδ+ neurons in EAc integrate convergent signals

Besides inputs from the LPBE, both BSTL and CeA are strongly innervated by the basolateral nucleus of the amygdala, especially its posterior subdivision (BLP) (Dong et al. 2001a; Pitkanen et al. 2003), and by the insular cortex (InsCx) (Saper 1982; Sun et al. 1994; Yasui et al. 1991a). Kim and colleagues (Kim et al. 2017) recently showed that BLP strongly targeted PKCδ+ neurons in CeL/C, and a study using rabies virus tracing unveiled convergent inputs to CeL PKCδ+ neurons from multiple brain regions including InsCx, BLP, and LPBE (Cai et al. 2014). However, it is not known if the same goes true for BSTLD PKCδ+ neurons and whether they can potentially integrate information from both intra-amygdaloid (i.e., BLP) and extra-amygdaloid (i.e., LPB or InsCx) inputs. We, thus, injected the anterograde tracer BDA in BLP or in InsCx and carried out triple fluorescent labeling in BSTLD and CeL/C to look for the potential innervation of PKCδ+ neurons by CGRP+ baskets (potentially from LPBE) and BLP or InsCx afferents.

The BDA injection sites in BLP were largely confined to the lateral part of the caudal BLP (Fig. 4a, b; bregma − 2.45 mm), with minor leakage in the nearby piriform cortex and lateral nucleus of amygdala. In the ipsilateral BSTL, BDA+ axon terminals spread quite evenly in BSTLD and BSTLP (Fig. 4c). At higher magnification, BDA+ axonal varicosities (Fig. 4d) could be observed at close appositions with PKCδ+ neurons that were also surrounded by CGRP+ basket-like terminals. Similarly, the CeA was also densely innervated by BDA+ axons from BLP (Fig. 4e). At cellular level, these BDA+ axonal varicosities in CeL/C could also form close apposition with PKCδ+ neurons contacted by CGRP+ baskets (Fig. 4f).

The BDA injections in InsCx targeted the granular and dysgranular insular areas at middle level (bregma − 0.23 mm), with some minimal extent dorsally in the secondary somatosensory cortex (S2) (Fig. 5a, b). Ipsilaterally, a moderate-to-strong projection was found in the BSTLD (Fig. 5c) and in the CeL/C (Fig. 5e), in the regions where intense CGRP+ axonal field and PKCδ+

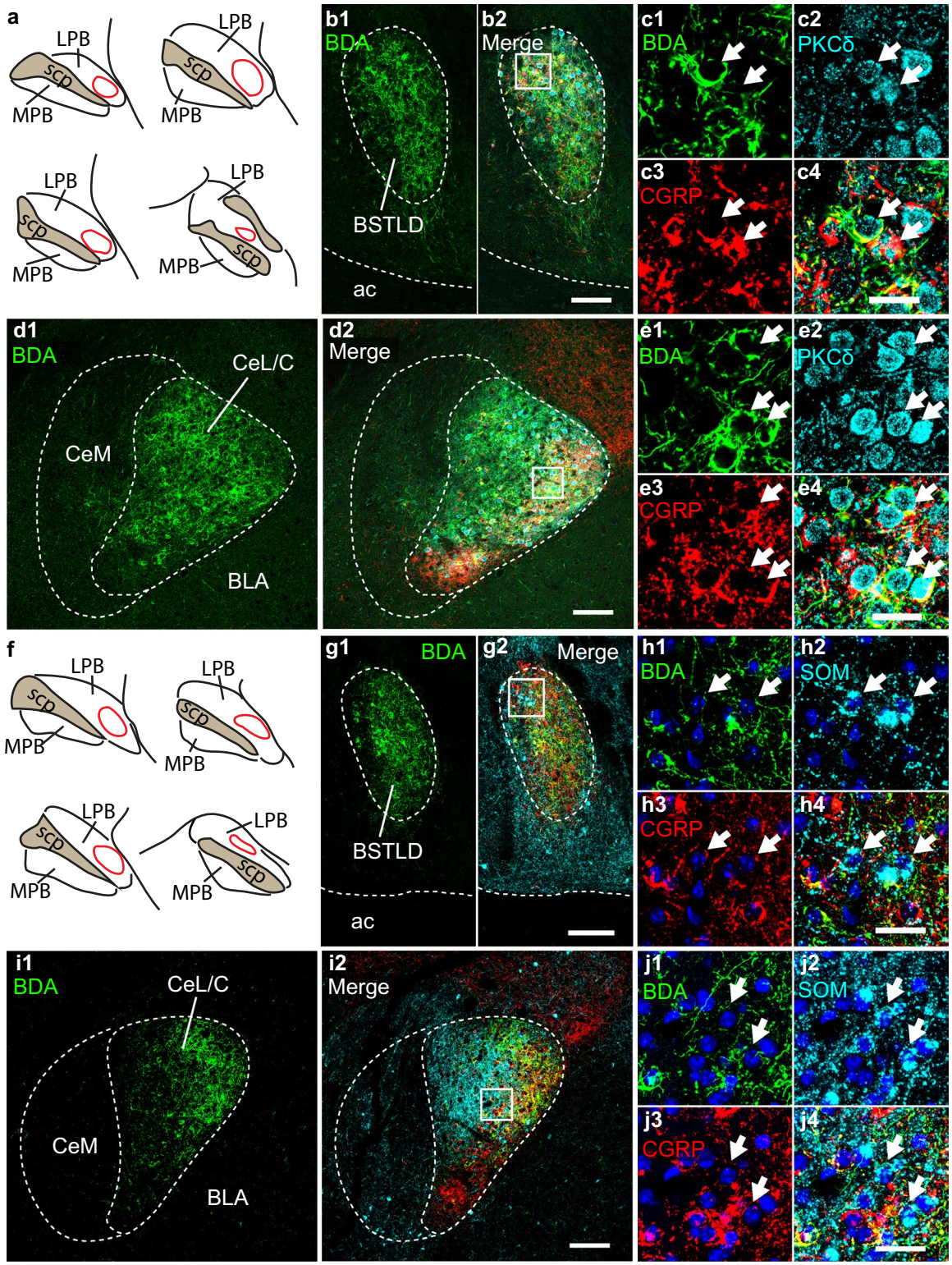

neurons coexisted. Observation at high magnification confirmed the existence of simultaneous axonal appositions by BDA+ varicosities and CGRP+ varicosities onto a single PKCδ+ neuron in BSTLD (Fig. 5d) and in CeL/C (Fig. 5f).

Thus, these structural evidences support the notion that PKCδ+ neurons in EAc can mediate the integration of both viscero- and somato-sensory signals from LPBE and highly processed polymodal information from BLP and InsCx. However, it should be noted that these BLP and InsCx inputs

◂**Fig. 3** Structural apposition of CGRP+ terminals anterogradely labeled from LPB onto PKCδ+ neurons in BSTLD and CeL/C. Following BDA injection in the LPBE (a, f), triple labeling for BDA (green), CGRP (red) and PKCδ (cyan) (**b**–**e**), or for BDA (green), CGRP (red) SOM (cyan) along with DAPI (blue) (**g**–**j**) was performed on BSTLD (**b, c, g, h**) and CeL/C (**d, e, i, j**). The injection (red outlines) was centered in LPBE (**a, f**). Dense cores of BDA-labeled fibers were observed in BSTLD but not BSTLP (b1, g1) where they overlap with the distribution of CGRP+ and PKCδ+ (b2) or SOM+ (g2) somas and fibers. Similarly, BDA-labeled fibers were densest in CeL/C (d1, i1) and partially overlapped with the distribution of CGRP+ and PKCδ+ (d2) or SOM+ (i2) somas and fibers. In c1–c4 and e1–e4, the higher magnifications of the boxed areas in b2 and d2, respectively, show that BDA+ basket-like structures, either in CGRP+ or CGRP−, can be found in close apposition with PKCδ+ somas (arrows) in BSTLD (c1–c4) and CeL/C (e1–e4). In addition, BDA−/CGRP+ terminals can also contact PKCδ+ somas. In h1–h4 and j1–j4, the higher magnifications of the boxed areas in g2 and i2, respectively, show that BDA+ basket-like structures, either CGRP+ or CGRP− are rarely found in close apposition with SOM+ somas in BSTLD (h1–h4) and CeL/C (j1–j4). See list. Scale bars: b1–b2, 100 µm; c1–c4, 25 µm; d1–d2, 100 µm; e1–e4, 25 µm; g1–g2, 100 µm; h1–h4, 25 µm; i1–i2, 100 µm; j1–j4, 25 µm

onto PKCδ+ neurons are not exclusive, as numerous BDA+ varicosities were observed without evident apposition to PKCδ+ neurons in BSTLD and CeL/C.

A majority of CeM-projecting or BSTLV-projecting neurons in BSTLD and CeL/C express PKCδ

After establishing the structural evidences for possible integration of sensory and polymodal pathways onto PKCδ+ neurons, we asked what the possible downstream targets of these neurons are in the EAc. Both BSTLV and CeM, which are considered as the main output subnuclei of the EAc, have long been known as important intrinsic targets of BSTLD and CeL/C (Cassell et al. 1999; Dong et al. 2001b). It has been shown that PKCδ+ neurons in the CeL/C project to CeM (Haubensak et al. 2010; Li et al. 2013), but the neurochemical organization of connections inside the BSTL and between CeA and BSTL is still elusive. We thus injected the retrograde tracer CTb into the CeM (Fig. 6) or the BSTLV (Fig. 7), followed by triple fluorescent labeling for neuronal markers.

CTb injections ($n = 3$) in rostral CeM (bregma level: − 0.95/− 1.07 mm) were centered in its ventral or dorsal portions (Fig. 6a), based on the cytoarchitectural features in DAPI staining (Fig. 6b) and the observation of typical retrograde labeling in rostral lateral amygdala (LA) and InsCx. In these cases, a robust retrograde labeling was found in the CeL/C (Fig. 6f, g), while much fewer cells were labeled in BSTLD (Fig. 6d, e). Quantitative analysis of the co-localization between CTb and PKCδ or SOM immunoreactivity revealed that, among the CeM-projecting neurons in CeL/C, 71.4 ± 1.3% (Mean ± SEM) were PKCδ+ and 13.9 ± 2.4% were SOM+ (two-sample t test, p value = 0.0009). In comparison, 60.8 ± 1.5% of CTb+ cells in BSTLD were PKCδ+, but only 19.2 ± 2.6% of them were SOM+ (two-sample t test, p value = 0.002).

CTb injections ($n = 3$) into BSTLV area (including the fusiform nucleus) (Fig. 7a, b) revealed a considerable number of labeled neurons in BSTLD and CeL/C. The injection cores were confined to BSTLV as judged by DAPI staining, and a few/no retrograde labeling occurred in the BSTMA and medial amygdaloid nucleus (MeA). In BSTLD, we found that 64.6 ± 4.1% (Mean ± SEM) of CTb+ neurons were PKCδ+, while only 5.1 ± 0.1% of them were SOM+ (two-sample t test, p value = 0.011). In CeL/C, 48.1 ± 0.6% of BSTLV-projecting neurons were PKCδ+, by contrast only 2.7 ± 0.2% were SOM+ (two-sample t test, p value = 0.048).

Taken together, our data suggest a significant role of PKCδ+ neurons in relaying information flow within EAc from BSTLD and CeL/C to BSTLV and CeM. However, a sizeable part of the projections from BSTLD and CeL/C to BSTLV and CeM may originate in PKCδ/SOM neurons.

Both PKCδ+ and SOM+ neurons are involved in BSTLD-CeL/C reciprocal connections

Although BSTL and CeA have been known to be reciprocally connected to each other (Dong et al. 2001a; Gungor et al. 2015; Sun and Cassell 1993; Sun et al. 1991, 1994), it remains unclear which cell type mediates the mutual connections between BSTLD and CeL/C. In mouse, rabies virus tracing from CeL PKCδ+ neurons revealed a dense neuronal labeling in dorsal BSTL (Cai et al. 2014), which arose an interesting speculation that PKCδ+ cells might serve as intrinsic projection neurons between BSTLD and CeL/C. To test this hypothesis, we carried out retrograde (Fig. 8) and anterograde (Fig. 9) tracings from BSTLD and CeL/C, followed by immunostaining of the tracers, PKCδ and SOM.

To determine if PKCδ+ and/or SOM+ neurons in CeL/C project to BSTLD, CTb was injected in BSTLD area ($n = 2$; bregma level + 0.13 mm). The injection sites were restricted to the BSTL region containing PKCδ+ neurons, corresponding to the BSTLD (Fig. 8 b, c) and led to a large number of retrogradely labeled neurons in CeM and CeL/C, while labeling in medial amygdala was rarely seen (Fig. 8d). With confocal analysis, we found both CTb+/PKCδ+ and CTb+/SOM+ double-labeled neurons in ipsilateral CeL/C (Fig. 8e). In a similar attempt, we labeled CeA-projecting neurons in BSTLD by injecting retrobeads into caudal CeL/C ($n = 2$; Fig. 8f, g). Here, the retrobeads were preferred to CTb to avoid any leakage in the CeM. Retrobeads, indeed, produced a local injection zone in CeL/C, without extension into CeM (Fig. 8g). Despite a leakage along the micropipette track into the amygdalostriatal transition area (ASt) and globus pallidus (GP), we considered that, possible confounding,

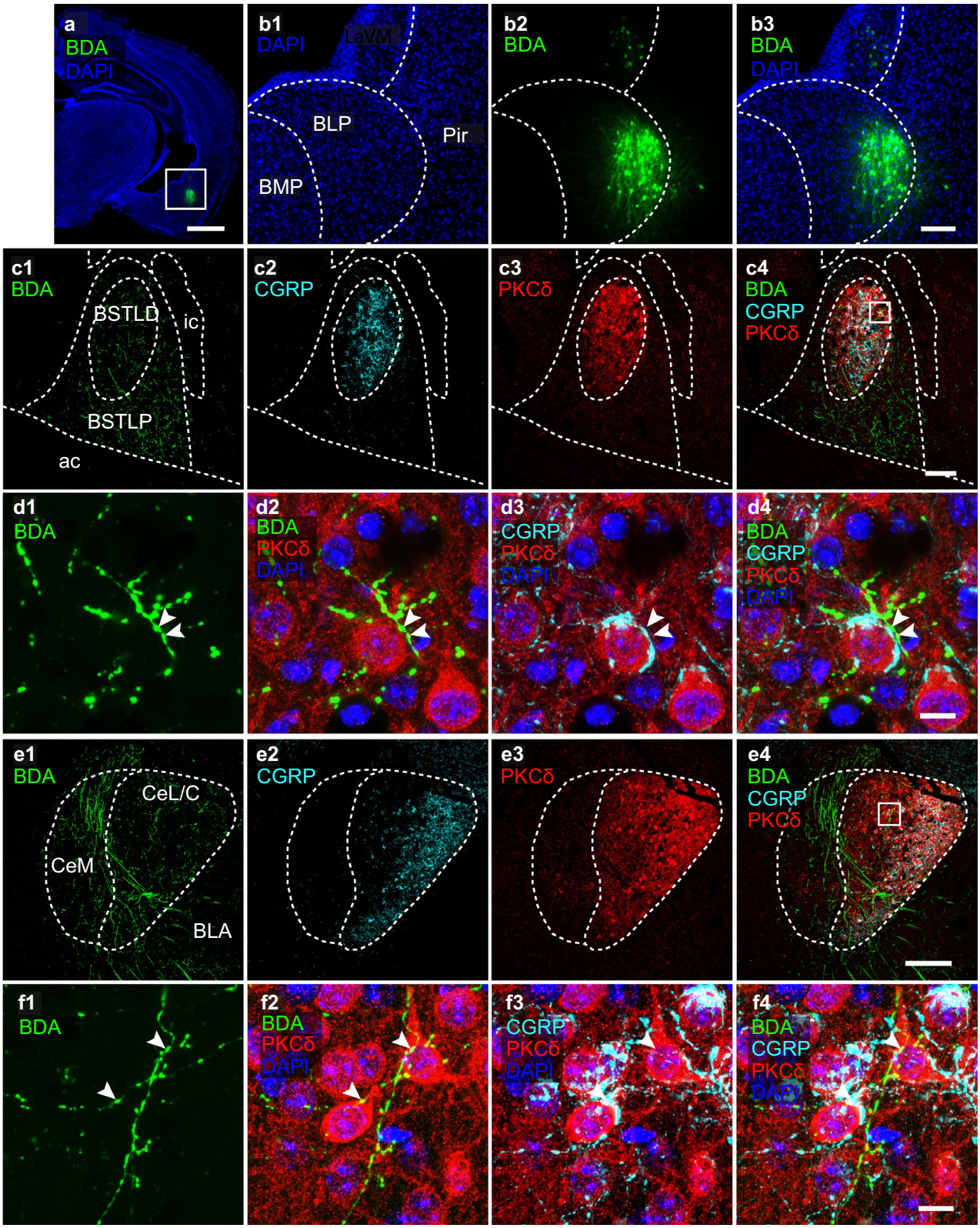
a
BDA
DAPI
b1
DAPI
LaVM
BLP
Pir
BMP
b2
BDA
b3
BDA
DAPI
c1
BDA
BSTLD
ic
BSTLP
ac
c2
CGRP
c3
PKCδ
c4
BDA
CGRP
PKCδ
d1
BDA
d2
BDA
PKCδ
DAPI
d3
CGRP
PKCδ
DAPI
d4
BDA
CGRP
PKCδ
DAPI
e1
BDA
CeL/C
CeM
BLA
e2
CGRP
e3
PKCδ
e4
BDA
CGRP
PKCδ
f1
BDA
f2
BDA
PKCδ
DAPI
f3
CGRP
PKCδ
DAPI
f4
BDA
CGRP
PKCδ
DAPI

◂**Fig. 4** Projections from caudal BLP and from CGRP+ terminals can target the same PKCδ+ neuron in BSTLD and CeL/C. After anterograde tracing from the caudal BLP area (**a, b**; bregma level −2.45 mm), triple immunofluorescence labeling of BDA (green), CGRP (cyan), and PKCδ (red), together with nuclear counterstaining by DAPI (blue), was performed on BSTL (**c, d**) and CeA sections (**e, f**). BDA injections were located in lateral region of the caudal BLP, with minor leakage in the nearby piriform cortex (Pir) and ventromedial part of the lateral nucleus of amygdala (LaVM) (b1–b3). BDA+ axon were present in most of the BSTL, and overlapped in BSTLD with PKCδ+ neurons and CGRP+ terminals. At high magnification, z-projection images (z stack = 5.43 µm) revealed close apposition of BDA+ axonal varicosities (d1, d2, d4; arrowheads) onto CGRP-innervated PKCδ+ neurons (d4). Similarly, moderate-to-dense labeling of BDA+ axonal terminals was observed in CeL/C, overlapping with CGRP+ axonal field and PKCδ+ neuronal populations. z-Projection images (z stack = 9.38 µm) showed close apposition of BDA+ axonal varicosities (f1, f2, f4; arrow heads) onto PKCδ+ neurons innervated by CGRP+ axonal terminals. Abbreviations: see list. Scale bars: **a**, 1.0 mm; **b**, 150 µm; c1–c4, 100 µm; d1–d4, 10 µm; e1–e4, 150 µm; f1–f4, 10 µm

retrograde labeling in BSTLD would be negligible as anterograde tracing from BSTLD rarely labeled axons in ASt region. In this case, similar to that of CeL/C, the retrograde labeling could be found in both PKCδ+ neurons (Fig. 8j) and SOM+ neurons (Fig. 8i).

Thus, our evidences indicate that both PKCδ+ and SOM+ neurons contribute to intra-EAc connections, mediating mutual talks between the BSTLD and CeL/C. To further identify the possible neurochemical profile of the neurons that receive inputs from BSTLD or CeL/C, we injected PHA-L in BSTLD or CeL/C and looked for potential appositions of anterogradely labeled axons with PKCδ+ and SOM+ neurons (Fig. 9).

A small PHA-L injection into BSTL produced a restricted labeling of neurons and processes, confined to the PKCδ-expressing BSTLD (Fig. 9b). In caudal CeA, a moderate density of PHA-L+ axonal branches and terminals were found in CeM and CeL/C (Fig. 9c). Confocal images (z stack = 11.9 µm) at high magnification showed that PHA-L+ varicosities from single continuous axons ramifications could be found apposed to both PKCδ+ and SOM+ neurons (Fig. 9d). Similarly, PHA-L injection sites into caudal CeL/C were centered in CeL/C, without leakage in BL or CeM ($n = 1$; Fig. 9f). Numerous PHA-L+ axons could be observed in BSTL, with the highest density in the BSTLD (Fig. 9 g). Apposition analysis following triple immunofluorescence staining revealed that many axon terminals formed close appositions with PKCδ+ and SOM+ neurons (Fig. 9h).

Thus, we concluded that projections from PKCδ+ and SOM+ neurons in BSTLD and CeL/C can target both PKCδ+ and SOM+ in the same subdivisions.

SOM+ neurons in BSTLD and CeL/C are the main sources of downstream projections to brainstem

Apart from intra-EAc projections, neurons in BSTLD and CeL/C give rise to efferent to extra-EAc targets, as well, including the LPB and the PAG (Dong et al. 2001b; Gray and Magnuson 1992; Moga and Gray 1985; Petrovich and Swanson 1997; Tokita et al. 2009). Interestingly, brainstem-projecting neurons in BSTL and CeA share similar neuropeptidergic features in rats (Moga et al. 1989). In mice, it has been shown that SOM+ cells in CeL/C project to PAG (Penzo et al. 2014). To establish the neurochemical identity of neurons in BSTLD and CeL/C projecting to brainstem, we injected retrograde tracers into LPB and PAG.

Fluorogold (FG) injections in LPB ($n = 3$; Fig. 10) were centered within LPBE (bregma—5.19 mm) and extended diffusely into other subdivisions of LPB (Fig. 10b). The retrograde labeling in BST and amygdala was specifically restricted to BSTL and CeA, especially in BSTLD and CeL/C, with much sparser labeling in BSTLP and CeM. In BSTLD (Fig. 10d, e) as in CeL/C (Fig. 10f, g), numerous FG+ cells were SOM+ but very few were PKCδ+. Quantitative analysis (Fig. 10c) revealed that, SOM+ neurons accounted for 62.7 ± 0.4% and 63.9 ± 0.7% of the retrogradely labeled cells in BSTLD and CeL/C, respectively, whereas only 6.1 ± 0.4% (BSTLD) and 6.9 ± 0.7% (CeL/C) of FG+ neurons were PKCδ+ (two-sample t test, BSTLD p value = 0.011, CeL/C p value = 5.37e−06).

To further examine the possibility that BSTLD and CeL/C projections to LPBE can target CGRP+ neurons, we processed sections from animals with PHA-L injections into BSTLD (same case as in Fig. 9b) or into CeL/C (same case as in Fig. 9f), to label PHA-L and CGRP on LPB sections. Consistent with the previous retrograde tracing, intense labeling of PHA-L+ axons was observed in LPB, especially dense in LPBE, following PHA-L injection in BSTLD (Fig. 11b) or CeL/C (Fig. 11d). CGRP+ neurons were concentrated in the ventrolateral part of the LPB, including the LPBE. Confocal analysis at high magnification revealed frequent, although not exclusive, appositions between PHA-L+ axonal varicosities, from BSTLD and CeL/C, and LBPE somas containing CGRP immunofluorescence (Fig. 11b, d).

To investigate the EAc projection to PAG, we used retrograde tracers FG or CTb and performed triple immunofluorescence staining for the tracer, PKCδ and SOM. To achieve reasonable number of retrograde labeling in BSTLD and CeL/C (versus BSTLP or CeM), we produced large injection sites with tracer deposits extending into the lateral (LPAG) and ventrolateral (VLPAG) columns of the PAG and dorsal raphe nuclei (DR; bregma −4.47/−4.59 mm; Fig. 12b, c). Retrogradely labeled cells were found in BSTL and CeA, including BSTLD (Fig. 12d) and CeL/C (Fig. 12f). While no quantification has been done (one FG case and one CTb

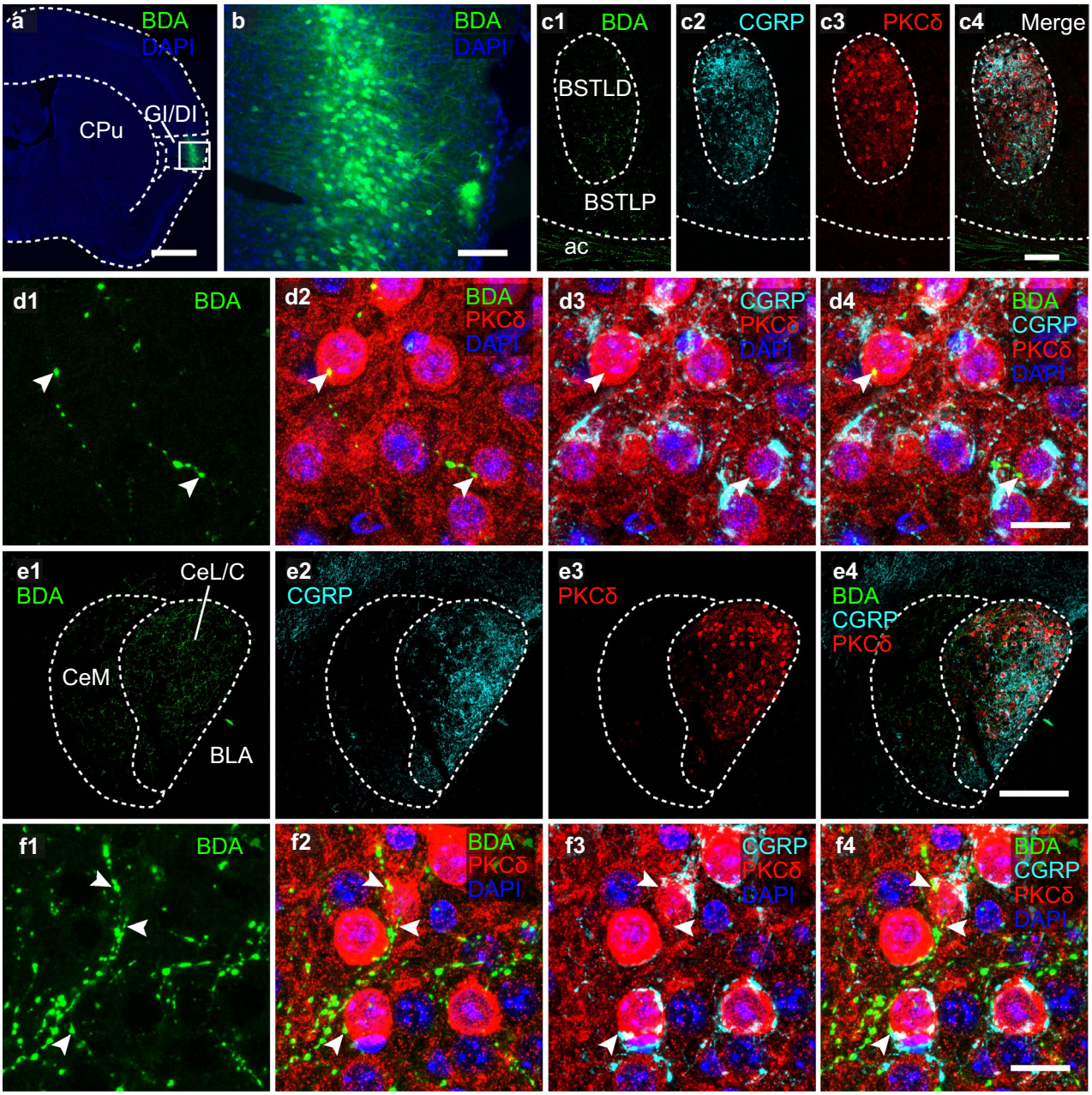

Fig. 5 Projections from InsCx and from CGRP+ terminals can target the same PKCδ+ neuron in BSTLD and CeL/C. Following anterograde tracing from InsCx (**a, b**; bregma level −0.23 mm), triple immunofluorescence labeling of BDA (green), CGRP (cyan), and PKCδ (red), together with nuclear counterstaining by DAPI (blue), was performed on BSTL (**c, d**) and CeA sections (**e, f**). BDA injections were restricted to in layer II/III of InsCx and largely confined to granular (GI) and dysgranular (DI) areas (**a, b**; epifluorescence images by NanoZoomer S60). The BDA+ axons spread in all the BSTL, including BSTLD where it overlapped with PKCδ+ neurons and CGRP+ terminals (c1–c4; single confocal plane). With high magnification, z-projection images (z stack = 8.89 µm) revealed close apposition of BDA+ axonal varicosities (d1, d2, d4; arrow heads) onto CGRP-innervated PKCδ+ neurons (d4). Similarly, BDA+ axonal terminals were also found in CeL/C, which again largely coincides with CGRP+ axonal field and PKCδ+ neuronal populations (e1–e4; z stack = 5.93 µm). Higher magnification revealed close apposition of BDA+ axonal varicosities (arrow heads) onto PKCδ+ neurons surrounded by CGRP+ basket-like terminals (f1, f2, f4; z stack = 9.38 µm). See list. Scale bars: **a**, 1.0 mm; **b**, 100 µm; c1–c4, 100 µm; d1–d4, 15 µm; e1–e4, 200 µm; f1–f4, 15 µm

case), we observed that more than half of the retrogradely labeled neurons co-localized with SOM immunofluorescence in BSTLD (Fig. 12e) and in CeL/C (Fig. 12g), but almost never with PKCδ signal. These data suggest that, in both BSTLD and CeL/C, SOM+, but not PKCδ+ neurons, project to PAG/DR areas.

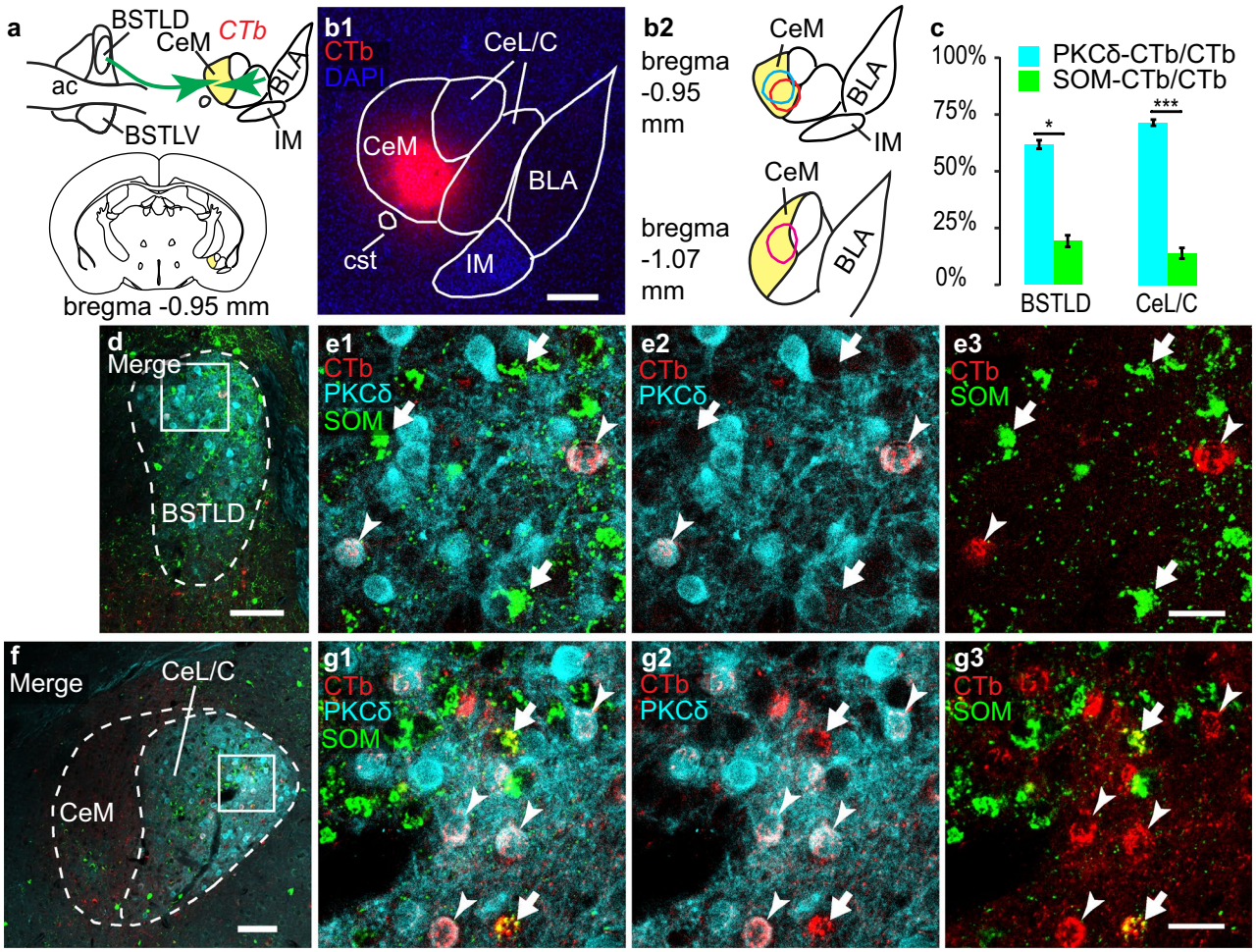

Fig. 6 Retrogradely labeled CeM-projecting neurons in BSTLD and CeL/C express PKCδ. After injection of the retrograde tracer CTb into rostral CeM (**a, b**, bregma − 0.95 mm), triple labeling of SOM (green), PKCδ (cyan) and CTb (red) was performed on BSTLD (**d, e**) and CeL/C sections (**f, g**). The injection sites ($n=3$; **b1, b2**) were confined to the rostral CeM, with minimal extension into nearby regions. **c** Percentages of CTb+ somas positive for PKCδ and SOM in the BSTLD (PKCδ 60.8 ± 1.5%; SOM 19.2 ± 2.6%; two-sample t test, $p<0.05$) and CeL/C (PKCδ 71.4 ± 1.3%; SOM 13.9 ± 2.4%; two-sample t test, $p<0.001$). Confocal imaging in the BSTLD (**d**) and CeL/C (**f**) shows that retrogradely labeled CTb+ neurons were frequently PKCδ+ (e1, e2, g1, g2; arrowheads), but rarely SOM+ (e1, e3, g1, g3; short arrows). Abbreviations: see list. Scale bars: b1, 250 µm; **d**, 100 µm; e1–e3, 25 µm; **f**, 100 µm; g1–g3, 25 µm

Taken together, these data support a major role of BSTLD and CeL/C SOM+ neurons in mediating long-range projections to LPB and PAG, while PKCδ+ neurons contribute very little to these outputs.

Discussion

In this study, we addressed the structural organization of specific cell-type neuronal circuits in BSTL and CeA of mice, by combining retrograde and anterograde tract tracing with immunofluorescence staining. Overall, we looked at the similarities of (1) the long-range external inputs, (2) intrinsic projections, and (3) long-range external outputs. We propose a model of cell-type specific parallel microcircuits in BSTL and CeA, based on the connectivity of PKCδ+ and SOM+ neuronal populations (Fig. 13).

For external inputs, our data support the hypothesis that multiple excitatory inputs can converge onto single neuronal populations in BSTLD and CeL/C. For instance, excitatory sensory information from cortex or polymodal information from amygdala nuclei (i.e., BLP) can converge to PKCδ+ neurons which are also innervated by excitatory CGRP+ sensory inputs from brainstem (i.e., LPB). These excitatory drives onto distinct neuronal populations in EAc are then processed by intrinsic inhibitory circuits, including local connections (i.e. SOM+ → SOM+ in CeL/C) (Douglass et al. 2017; Hunt et al. 2017) and long-range connections from CeA subdivisions (i.e., PKCδ+ neurons in CeL/C →BSTLV). Although cell-type

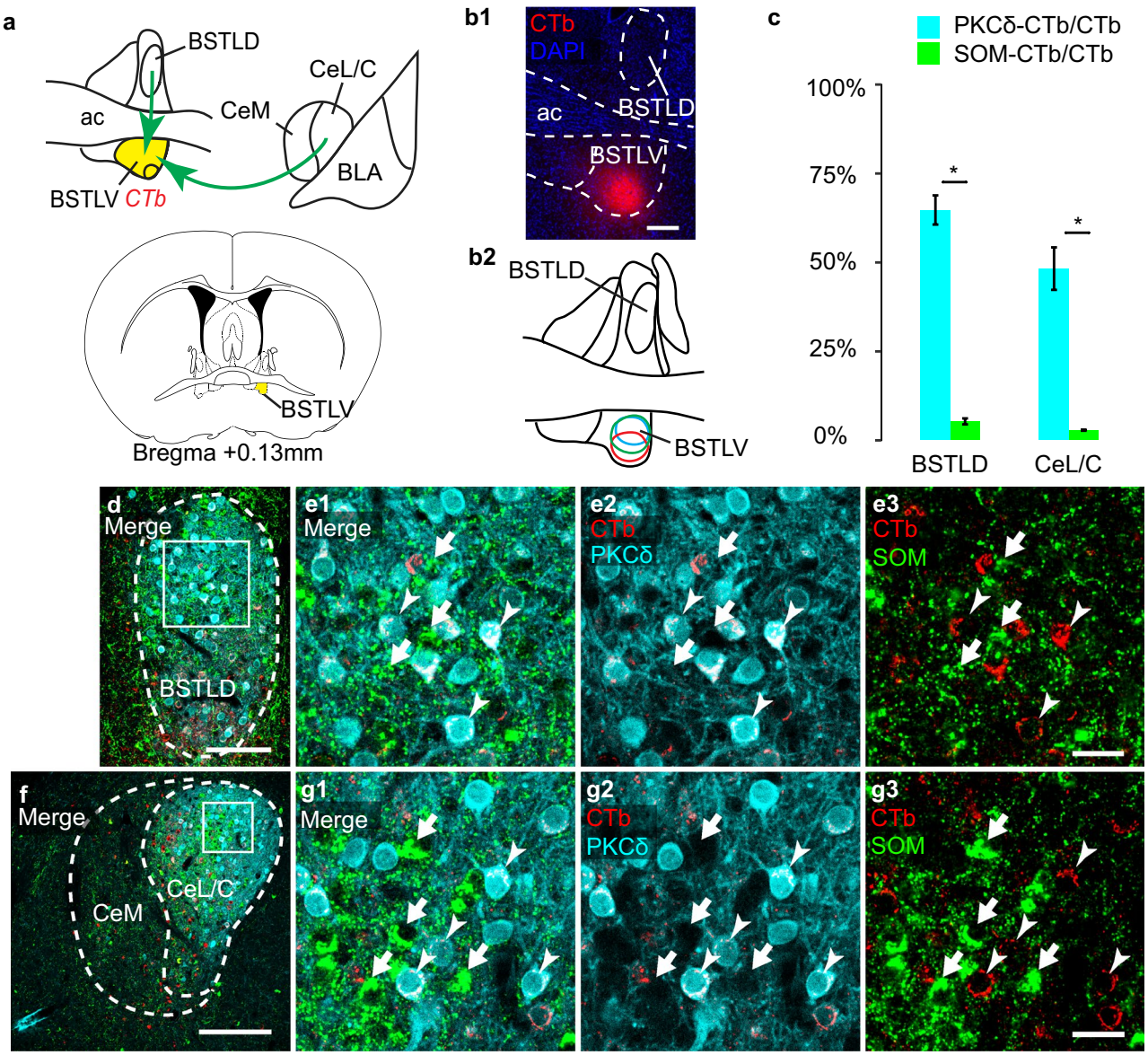

Fig. 7 Retrogradely labeled BSTLV-projecting neurons in BSTLD and CeL/C express PKCδ. After injection of the retrograde tracer CTb into anterior BSTLV (**a, b**, bregma + 0.13 mm), triple labeling of SOM (green), PKCδ (cyan), and CTb (red) was performed on BSTLD (**d, e**) and CeL/C sections (**f, g**). The injection sites ($n = 3$; b1–b2) were confined to the BSTLV with minimal extension to nearby areas. **c** Percentages of CTb+ somas positive for PKCδ and SOM in the BSTLD (PKCδ 64.6 ± 4.1%; SOM 5.1 ± 0.1%; two-sample t test, $p < 0.05$) and CeL/C (PKCδ 48.1 ± 0.6%; SOM 2.7 ± 0.2%; two-sample t test, $p < 0.05$). Confocal imaging in the BSTLD (**d**) and CeL/C (**f**) shows that retrogradely labeled CTb+ neurons were frequently PKCδ+ (e1, e2, g1, g2; arrowheads), but rarely SOM+ (e1, e3, g1, g3; short arrows). Abbreviations: see list. Scale bars: b1, 200 µm; **d**, 100 µm; e1–e3, 25 µm; **f**, 200 µm; g1–g3, 25 µm

specific circuit configurations in BSTLD remain to be explored, we hypothesize that similar configurations also exist there (dashed line, Fig. 13), which are featured with both heterotypic (SOM+ → PKCδ+; Fig. 13) and homotypic (i.e., SOM+ → SOM+; not shown) connections. We do confirm, however, the similar preferential innervations of BSTLV and CeM by PKCδ+ neurons in BSTLD and CeL/C, although sparse innervation from SOM+ populations was observed. We also found that the long-range, mutual, connections between BSTLD and CeL/C are carried out by both types of neurons. Finally, long-range external projection from BSTLD and CeL/C are carried out mainly by SOM+ neurons. Notably, we find that SOM+, but not PKCδ+, populations, mediate the output to LPBE and PAG. Taken together, we present structural evidence highlighting novel cell-type specific microcircuits in BSTLD, which are similarly configured as that of CeA.

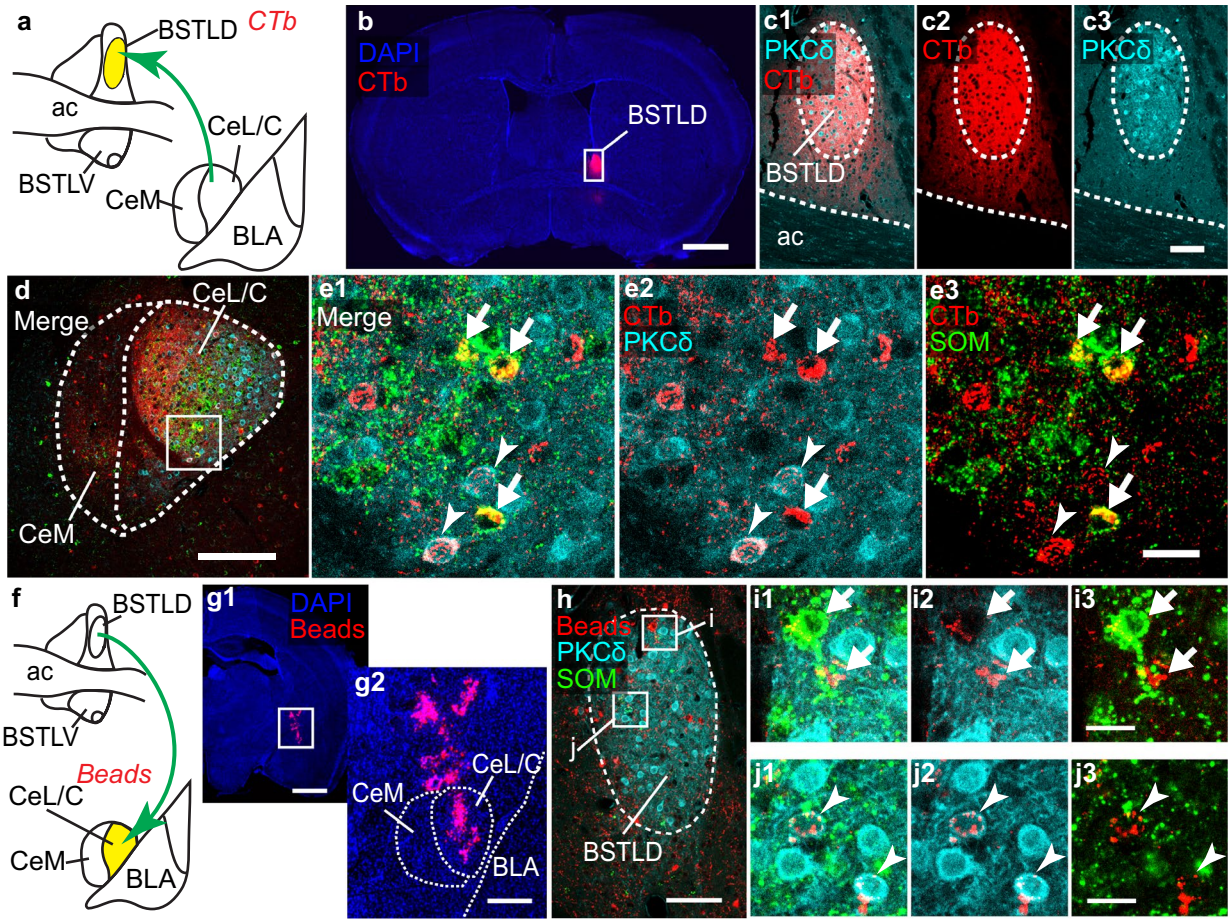

Fig. 8 Retrogradely labeled BSTLD- and CeL/C-projecting neurons express PKCδ or SOM. Following by CTb injection in BSTLD (**a**–**c**, bregma level + 0.13 mm) or red retrobeads in CeL/C (**f, g**, bregma level − 1.43 mm), triple immunofluorescence labeling was carried out for CTb (red), PKCδ (cyan) and SOM (green), while intrinsic fluorescence from retrobeads was used. In BSTL, CTb injection site was limited to the PKCδ-expressing BSTLD (**b, c**). In ipsilateral caudal CeL/C (**c**), confocal image (z stack = 5.78 µm) identified CTb+/PKCδ+ colabeled neurons (arrowheads) and CTb+/SOM+ ones (short arrows) (e1–e3). Pressure injection of red retrobeads resulted in dense deposit in CeL/C (g1, g2). Subsequent co-localization analysis revealed double labeling from SOM+ populations (arrowheads) (i1–i3) and PKCδ+ ones (short arrows) (j1–j3). See list. Scale bars: **b**, 1.0 mm; c1–c3, 100 µm; **d**, 200 µm; e1–e3, 25 µm; g1, 1.0 mm; g2, 250 µm; **h**, 100 µm; i1–i3, 20 µm; j1–j3, 20 µm

Technical considerations

The quality of injection sites is critical for reliable and accountable observations drawn from tract-tracing experiments. Overall, we used FG/CTb and retrobeads for retrograde tracing and PHA-L/BDA for anterograde tracing. After checking the neuroanatomical localization of injection sites on successive coronal brain sections, we excluded cases with confounding spillovers. When applied by iontophoresis, CTb, BDA, and PHA-L reliably produced limited injection sites, usually confined to the limits of the target nucleus (i.e., see CTb injection into BSTLD, Fig. 8). Iontophoresis of FG into LPBE usually resulted in a core in LPBE and diffusion in the other subdivisions of LPB, but we found minimal contaminations from these non-LPBE subdivisions as suggested by minimal retrograde labeling in non-EAc subdivisions. In our hands, pressure injection of retrobeads in CeL/C usually resulted in well-restricted injection sites, but often with tracer deposits along the pipette track, in ASt, GP, or CPu. However, none of these areas are innervated by BSTLD, based on the literature (McDonald 1991; Weller and Smith 1982) and our results from retrograde tracing.

We relied on antibodies to determine the cellular identity of PKCδ+ and SOM+ neurons. Due to unknown reasons, we observed that the corresponding immunofluorescence signal in BSTLD and CeL/C was weaker than the one in thalamic PKCδ+ neurons and cortical or striatal SOM+ neurons in the same brain sections. Nevertheless, the primary antibody for PKCδ which we used was previously shown to detect most of the PKCδ+ neurons in a PKCδ-cre transgenic mouse line (Haubensak et al. 2010). The antibody against SOM gave a specific labeling of SOM-expressing neurons (Jhou

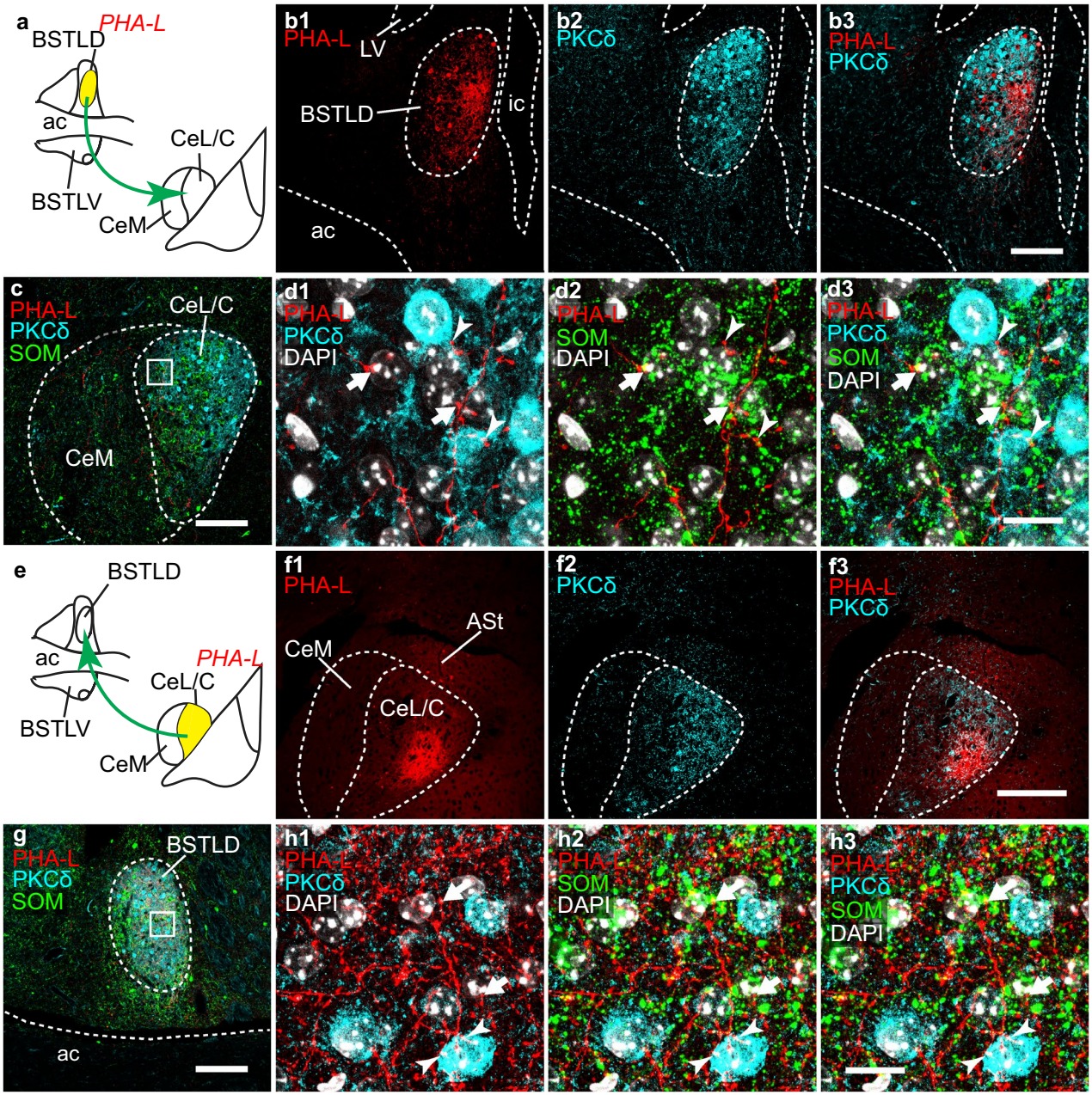

Fig. 9 Anterogradely labeled BSTLD or CeL/C axonal projections can target both PKCδ+ and SOM+ neurons. Following by PHA-L injection in BSTLD (**a, b**; bregma level + 0.01 mm) and in CeL/C (**e, f**; bregma level − 1.55 mm), triple immunofluorescence labeling was carried out for PHA-L (red), PKCδ (cyan) and SOM (green). In BSTL, restricted PHA-L injection site was confined to the BSTLD (b1–b3). In caudal level of CeL/C (**c**), confocal imaging (z stack = 11.9 µm) revealed PHA-L+ varicosities apposed to PKCδ+ (arrowheads) and SOM+ neurons (short arrows) (d1–d3). In another case, PHA-L injection into CeL/C (f1–f3) resulted in dense axonal labeling in BSTL, especially in BSTLD (**g**). With high magnification confocal images (z stack = 10.9 µm), PHA-L+ varicosities were observed forming close apposition with PKCδ+ (arrowheads) and SOM+ (short arrows) (h1–h3), see list. Scale bars: **b**, 150 µm; **c**, 150 µm; d1–d3, 15 µm; f1–f3, 200 µm; g, 150 µm; h1–h3, 15 µm

et al. 2009) but seems to reveal less neurons than what was observed in SOM-cre mouse line (Li et al. 2013). Finally, CGRP antibody revealed terminal fields in EAc that are largely consistent with the previous reports (Dobolyi et al. 2005). Thus, these tools allowed showing the basket-like CGRP+ axon terminals in appositions with PKCδ+ neurons in BSTLD and CeL/C, as PKCδ+ signal usually reliably labeled the whole cell body and proximal dendrites. We rarely observed these obvious basket-like terminals around SOM-expressing neurons. However, we can not exclude that

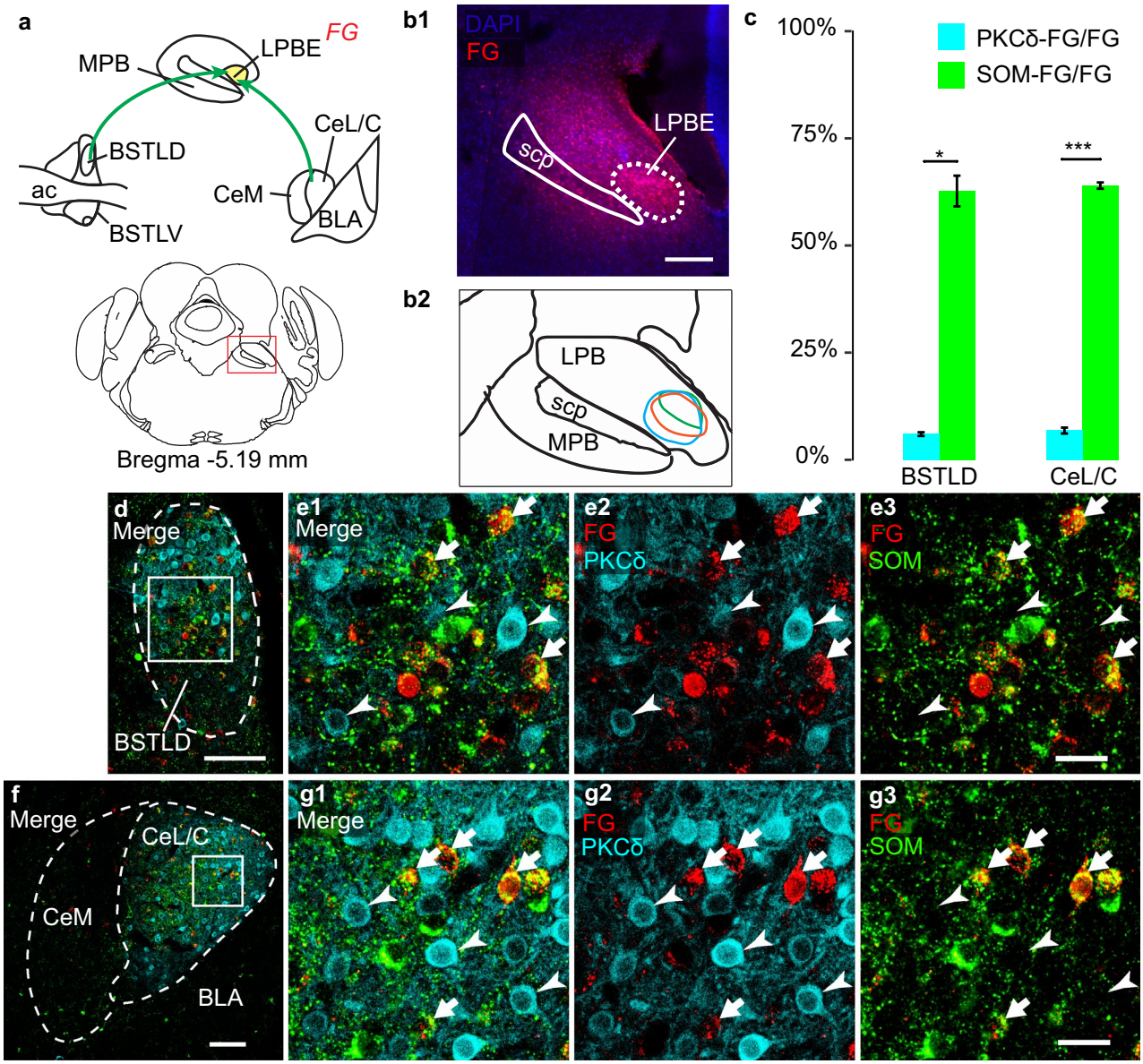

Fig. 10 LPBE-projecting neurons in BSTLD and CeL/C express mainly SOM. Triple labeling of FG (red), PKCδ (cyan) and SOM (green) in BSTLD (**d, e**) and CeA (**f, g**) was performed after FG retrograde tracing from LPBE (**a, b**, bregma level −5.19 mm). The FG injection sites ($n=3$) were centered in LPBE, with minor diffusion in the other LPB subdivisions (b1, b2). **c** Percentage of FG+ somas positive for PKCδ and SOM in BSTLD (PKCδ, 6.1 ± 0.4%; SOM, 62.7 ± 0.4%; p value < 0.05) and in CeL/C (PKCδ, 6.9 ± 0.7%; SOM, 63.9 ± 0.7%; p value < 0.001). d–g Confocal images show rare colabeling of PKCδ (arrowheads) with FG, whereas SOM+ neurons (short arrows) frequently contained FG, in both BSTLD (**d, e**) and CeL/C (**f, g**), see list. Scale bars: b1, 250 µm; **d**, 100 µm; e1–e3, 25 µm; **f**, 100 µm; g1–g3, 25 µm

more discrete thin CGRP+ terminals might contact SOM+ neurons at the level of soma or dendrites due to resolution limits. For the same reasons, we also likely underestimate the extent of CGRP+ contacts with PKCδ+ neurons as possible non-basket CGRP+ varicosities apposed with neurons are difficult to ascertain in our experimental conditions. The confirmation of CGRP+ synaptic contacts by immunostaining of synaptic markers or by synaptic ultra-structures via electron microscopy would be necessary in future studies.

Neurochemical features of EAc

The subdivisions of EAc have long been known to express a variety of neuropeptides and receptors, such as ENK, CRF, SOM, dopamine receptors, and serotonin receptors Htr2a (Cassell et al. 1986, 1999; De Bundel et al. 2016; Douglass et al. 2017; Veinante et al. 1997). In this study, we focused on the cellular connectivity of PKCδ+ and SOM+ neurons, primarily because these two neuronal

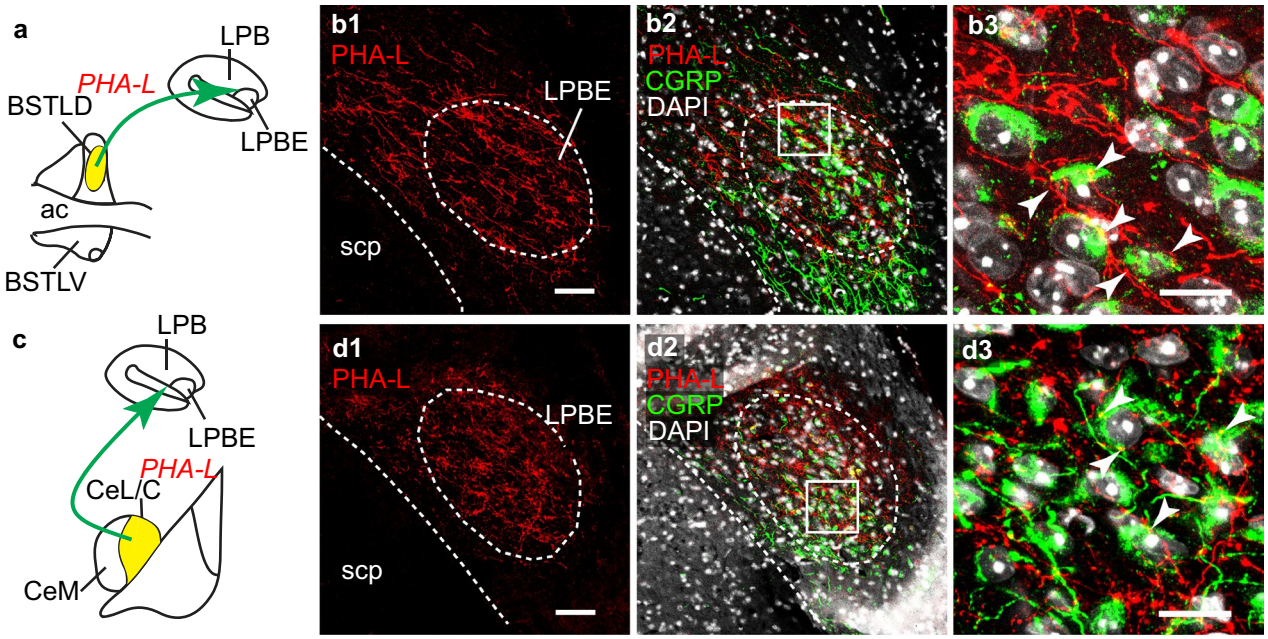

Fig. 11 BSTLD and CeL/C projections can target CGRP+ neurons in LPBE. Double immunofluorescence labeling for PHA-L (red) and CGRP (green), together with DAPI (white) in LPB, after PHA-L injection in BSTLD (**a**) or CeL/C (**c**). A dense PHA-L+ axonal labeling was observed in LPB, especially LPBE where it overlapped with the presence of CGRP+ neurons (b1, b2, d1, and d2). With high magnification confocal images, axonal appositions onto CGRP+ soma (arrowheads) were frequently observed for projections from BSTLD (b3; z stack = 9 µm) and CeL/C (d3; z stack = 7.9 µm), see list. Scale bars: b1–b2, 50 µm; b3, 15 µm; d1–d2, 50 µm; d3, 15 µm

populations are largely non-overlapping and constitute the majority of local GABAergic neurons in CeA (Haubensak et al. 2010; Li et al. 2013). Using double immunofluorescence staining, we found similar segregation and expression patterns of PKCδ and SOM in CeA than in a previous report using a cre transgenic mouse line (Li et al. 2013). In addition, we describe, for the first time, a similar expression pattern of PKCδ+ and SOM+ neurons in BSTLD. Even though immunofluorescence staining combined with the highly sensitive CARD method (Hunyady et al. 1996) allows us to visualize many SOM+ and PKCδ+ neurons in EAc, the transgenic mouse lines might provide a more robust and reliable way to label these neurons (Li et al. 2013).

On the other hand, these two neuronal populations can overlap with other neuronal markers. For example, more than 70% of PKCδ+ neurons in CeL/C and BSTLD coexpress the dopamine receptor D2 (D2R) in a Drd2-cre-EGFP mouse (De Bundel et al. 2016). PKCδ+ neurons do not overlap with Htr2a-expressing cells in CeL, but more than half of Htr2a+ neurons coexpress SOM (Douglass et al. 2017). SOM+ neurons in both BSTL and CeA can also coexpress neuropeptide Y (NPY) (Wood et al. 2016). Thus, it is possible that some of the EAc PKCδ+ and SOM+ neurons revealed in this study also belong to other specific neuronal populations.

Comparison with other studies on cell-type specific circuits in EAc

Long-range inputs

The neurochemical identities of presynaptic inputs from extra-EAc sources have been previously studied in various ways, especially those from LPBE and BLP, and are in accordance with our study. CGRP+ neurons in LPBE have been shown project to CeL/C or BSTL by immunohistochemistry (Dobolyi et al. 2005), retrograde tract-tracing (Carter et al. 2013), cell-type specific rabies tracing (Cai et al. 2014), and optogenetic mapping (Carter et al. 2013; Sato et al. 2015). Furthermore, CGRP receptor (CGRPR)-expressing CeL/C neurons were proved to be innervated by LPBE CGRP+ neurons, using a double cre mouse line (Han et al. 2015), while the connectivity of CGRPR+ neurons in BSTL remains relatively unexplored. In our study, most of the CGRP+ terminals in CeL/C and BSTLD, as well as many of the axon terminals anterogradely labeled from LPBE, appear as perisomatic basket-like terminals, morphologically similar to those described in studies on rat (Dobolyi et al. 2005; Sarhan et al. 2005) and mouse (Campos et al. 2016). We found a preferential targeting of CGRP+ terminals onto PKCδ+ somas and proximal dendrites, but not SOM+ ones.

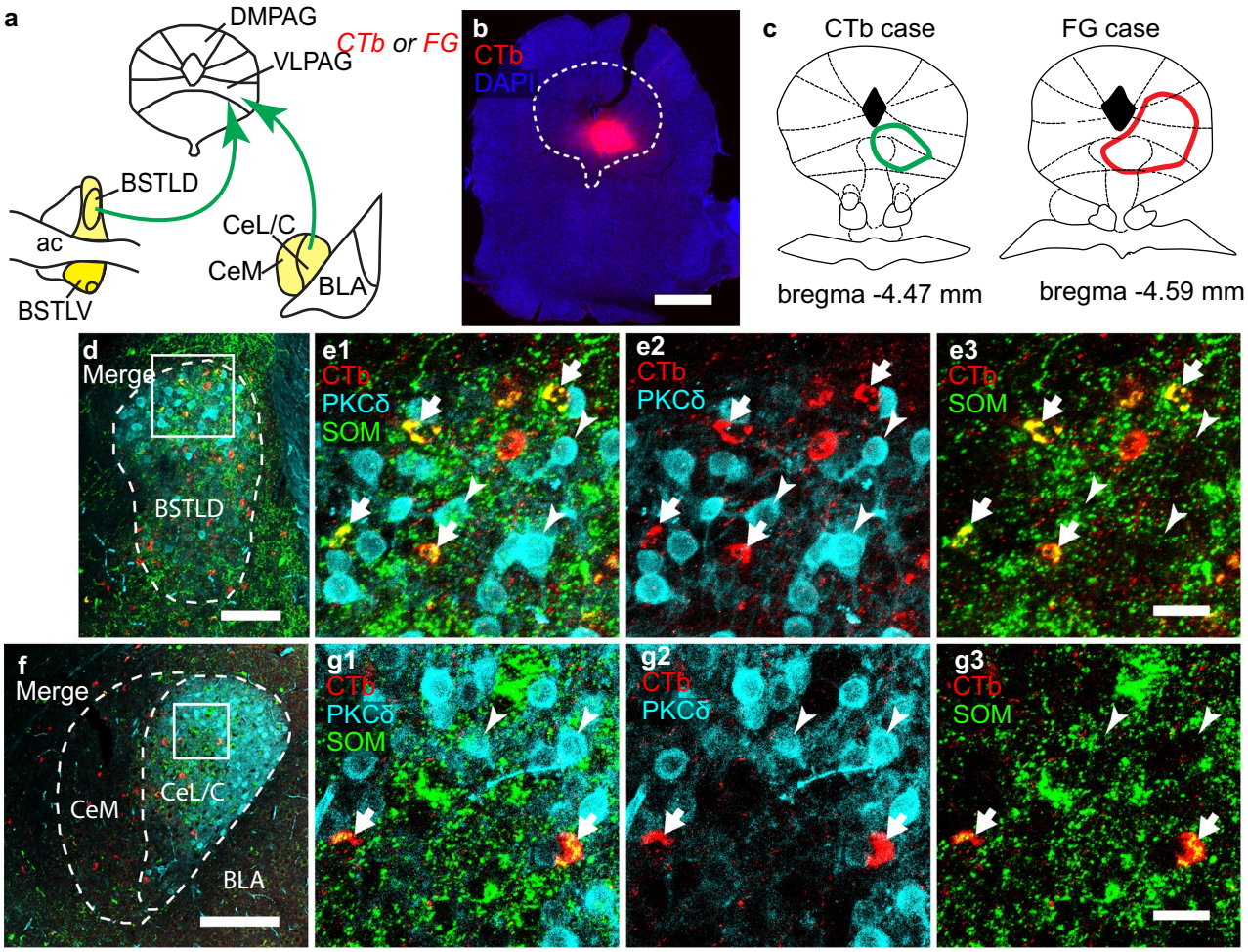

Fig. 12 PAG/DRN-projecting neurons in BSTLD and CeL/C express SOM. Triple labeling of CTb (red), PKCδ (cyan), and SOM (green) in BSTLD (**d, e**) and CeA (**f, g**), after CTb injection into PAG areas (**a**–**c**). **b** A CTb injection site. **c** The CTb and FG injection sites covered lateral (LPAG), ventrolateral PAG (VLPAG), and dorsal raphe (DR). **d, g** Confocal images show that most of the CTb+ neurons were colabeled by SOM (short arrows) in BSTLD (e1, e3; z-stack = 15.8 µm) and CeL/C (g1, g3; z-stack = 5.9 µm), but not PKCδ (arrowheads) in both areas (e1, e2, g1, g2). Abbreviations, see list. Scale bars: **b**, 1.0 mm; **d**, 100 µm; e1–e3, 25 µm; **f**, 200 µm; g1–g3, 25 µm

However, we cannot exclude a synaptic or extra-synaptic influence of CGRP on SOM+ neurons, as a recent study indicates that only about half of CGRPR+ neurons coexpress PKCδ in CeC of mice (Kim et al. 2017).

The projection from the basolateral nucleus of the amygdala (BL) to CeA and BSTL has been revealed by anterograde tract-tracing (Dong et al. 2001a; Pitkanen et al. 1995; Savander et al. 1996), monosynaptic rabies virus tracing (Kim et al. 2017), and optogenetic mapping (Li et al. 2013). It is worth noting that these CeA-projecting neurons are distributed differently along the rostral–caudal axis of the BL. Most of the CeA-projecting neurons are located in the caudal BL and express the protein phosphatase 1 regulatory subunit 1B (Ppp1r1b); while a minority, projecting essentially to CeC, expresses R-spondin 2 (Rspo2) (Kim et al. 2017). In line with these findings, we found that CTb tracing from BSTLD and CeL/C resulted in dramatically more labeling in BLP than anterior BL. Insular cortex inputs to CeA and BSTL have also been previously described (McDonald et al. 1999; Sun et al. 1994; Yasui et al. 1991a) and have been shown to arise mainly from agranular and dysgranular areas. In this study, we provide further evidences supporting a convergence of long-range pathways, from CGRP+ LPBE neurons and insular or BLP neurons onto individual PKCδ+ neuron in both BSTLD and CeL/C. However, this convergence is not exclusive to PKCδ+ cells as we also observed similar appositions to PKCδ− soma. The convergence of non-CGRP+ LPBE projections with other long-range inputs is also possible. It is also important to note that, even though we show that a number of given inputs can converge onto PKCδ+ population, other inputs might favor different neuronal populations. For example, it has been shown that

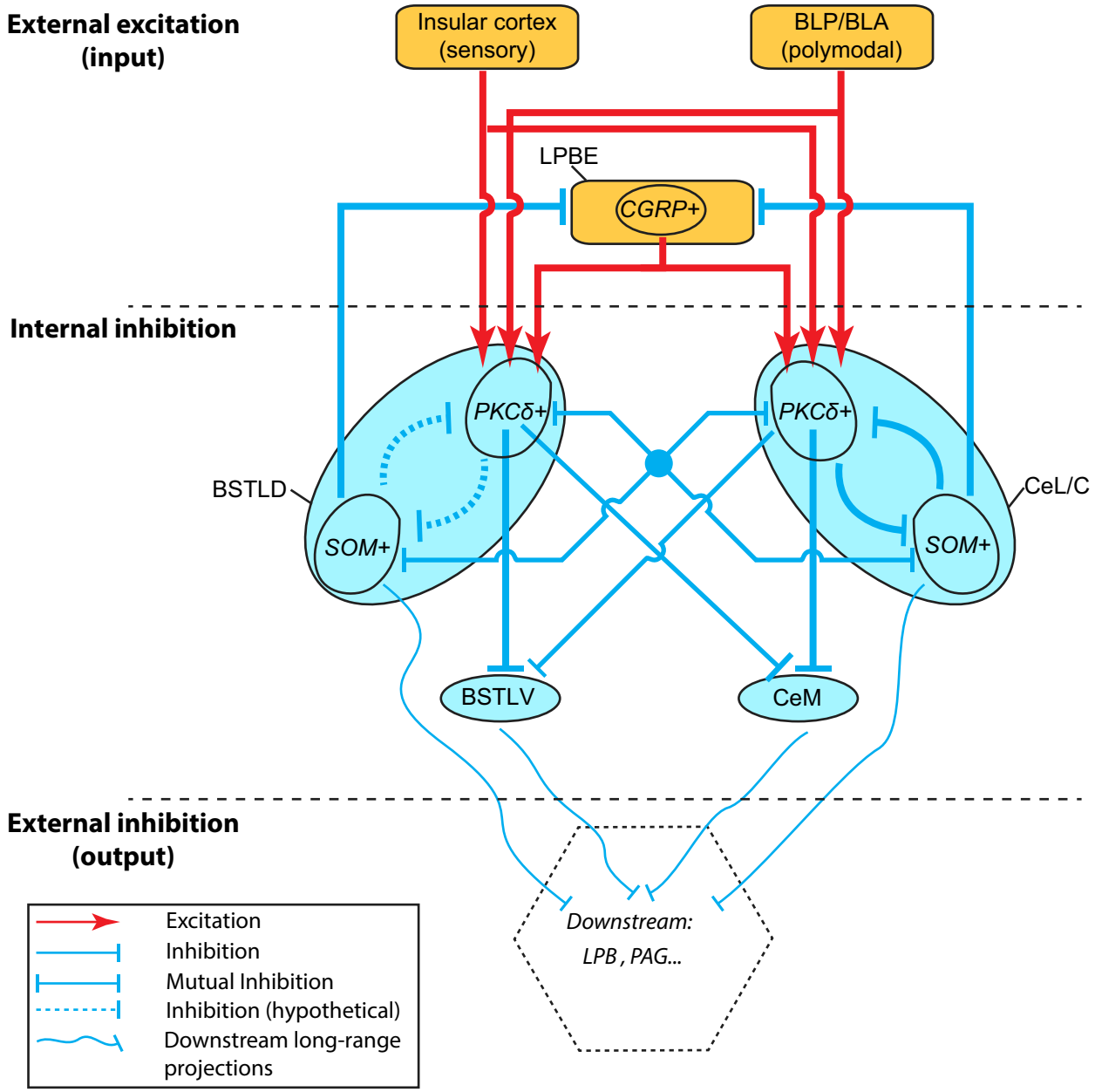

Fig. 13 A simplified model of parallel, cell-type specific, neuronal circuits in EAc. This model highlight the similar configuration of cell-type specific neuronal circuits in BSTL and CeA, based on PKCδ+ neurons and SOM+ neurons in BSTLD and CeL/C. Excitations coming from InsCx or basolateral amygdala nuclei, together with CGRP inputs from LPB, can converge onto PKCδ+ neurons in BSTLD and CeL/C, in a similar fashion. The internal inhibitory circuits in BSTLD or CeL/C are probably mediated by PKCδ+ and SOM+ neurons.. The internal long-range projections to BSTLV and CeM are primarily mediated by PKCδ+ neurons, while mutual connection between BSTLD and CeL/C can be mediated by both types, although the connection from CeL/C to BSTLD is stronger than that in reverse direction. The external inhibition to LPB and PAG can be mediated by SOM+ neurons in BSTLD or CeL/C, as well as undefined populations in BSTLV and CeM

afferents from the thalamic paraventricular nucleus target two times more the SOM+ neurons than PKCδ+ neurons in CeL/C (Penzo et al. 2015).

Intrinsic circuits

In this study, information concerning the local intrinsic connections (i.e., within BSTLD or CeL/C) is obscured by injection sites in bulk tract-tracing method. However, several recent works using genetic tools revealed complex

disinhibitory circuit between PKCδ+ and SOM+ neurons in the CeA. (Ciocchi et al. 2010; Douglass et al. 2017; Haubensak et al. 2010; Hunt et al. 2017; Janak and Tye 2015; Li et al. 2013). In the CeL/C, it has been shown that PKCδ+ neurons project to PKCδ− ones (Douglass et al. 2017; Haubensak et al. 2010) and that PKCδ− neurons are also interconnected (Hunt et al. 2017). By taking advantage of rabies virus tracing in multiple cre mouse lines, Kim and colleagues highlighted a surprising complexity in the connections between different neuronal populations in CeL, including those expressing PKCδ, SOM, CRF, neurotensin, and tachykinin 2 (Kim et al. 2017). Here again, information on BSTLD local circuits is still missing.

On the other hand, connections between EAc subdivisions, including short-range ones linking CeA or BSTL subdivisions and long-range ones between CeA and BSTL subdivisions, can be well resolved by restricted injection of retrograde tracer like CTb. Li and colleagues reported that about only 15% of CeM-projecting neurons are SOM+ in CeL/C (Li et al. 2013), while the majority of PKCδ+ neurons projects to CeM (Ciocchi et al. 2010; Li et al. 2013; Oh et al. 2014), which is consistent with our present findings. In comparison, limited information is available on BSTLV-projecting CeL/C or BSTLD neurons. We found that, similarly to the CeL/C-CeM pathway, PKCδ+ neurons are the main source of projection from the BSTLD to BSTLV with only a small contribution of SOM+ neurons. In addition, we also evidenced that similar proportion of these neuronal populations contribute to long-range projections from CeL/C to BSTLV and from BSTLD to CeM. It would be interesting to verify whether a single CeL/C or BSTLD neuron can project to both CeM and BSTLV, as it has been suggested for CeL neurons in rats (Veinante and Freund-Mercier 2003). While PKCδ+ neurons are clearly involved in these intrinsic EAc connections, it is worth noting that, in our hands, only about 80% of CeM-projecting neurons in BSTLD or CeL/C could be attributed to PKCδ and SOM population, while about 30–50% of BSTLV-projecting ones were not labeled by either of the two markers. This suggests that other neuronal populations can significantly contribute to the EAc intrinsic long-range projection, especially to BSTLV. Indeed, other neurochemically defined neuronal populations, such as NPY+ (Wood et al. 2016), Htr2a+ (Douglass et al. 2017), and CRF+ populations (Pomrenze et al. 2015), have been shown to mediate mutual or unidirectional connection between BSTL and CeA.

The cellular identity of neurons mediating BSTLD–CeL/C mutual connections is also elusive. We showed by retrograde and anterograde tracing that both PKCδ+ and SOM+ neurons can be the sources and the targets of the BSTLD-CeL/C connections (Fig. 9). Considering the fact that, in the CeL/C, PKCδ+ and SOM+ neurons preferentially target PKCδ− and SOM− neurons, respectively (Haubensak et al. 2010; Li et al. 2013), it is possible that the same cross-connectivity exists between CeL/C and BSTLD and that, for example, CeL/C PKCδ+ neurons preferentially inhibit BSTLD PKCδ−, including SOM+, neurons. The reciprocal may be also true, even though we observed that retrograde labeling in BSTLD was much weaker than that in CeL/C, indicating a preferential CeL/C → BSTLD direction.

Long-range outputs

EAc neurons projecting to LPB have been suggested to contain several different neuronal markers such as CRF, neurotensin, ENK, and SOM (Magableh and Lundy 2014; Moga and Gray 1985; Moga et al. 1989; Panguluri et al. 2009). While no or, only a faint, projection to LPBE from PKCδ+ neurons has been demonstrated by optogenetic mapping (Douglass et al. 2017; Oh et al. 2014), a strong terminal field from CeL/C PKCδ+ neurons was described in LPB (Cai et al. 2014). Our results rather indicate a preferential innervation of LPB by SOM+, not by PKCδ+, neurons, in both BSTLD and CeL/C. Furthermore, we showed by anterograde tracing that the axonal varicosities from EAc can specifically target CGRP+, as well as CGRP− neurons in LPBE.

Similarly, PAG-projecting neurons in BSTL and CeA have been known to express multiple neuronal markers such as neurotensin, CRF, and SOM (Gray and Magnuson 1992). In CeL/C, SOM+ neurons, but not PKCδ+ ones, have been shown to project to PAG by tract-tracing in SOM-cre mouse line (Penzo et al. 2014). So far, our findings on PAG/DR-projecting neurons are consistent with what has been reported for CeA and suggest that the same organization may exist in the BSTLD–PAG pathway. Besides LPB and PAG, CeL/C SOM+ neurons can also project to the solitary nucleus (Sol) (Gray and Magnuson 1987; Higgins and Schwaber 1983) and to the paraventricular thalamic nucleus (Penzo et al. 2014). Taken together, it is reasonable to hypothesize that SOM+ neurons, not PKCδ+ ones, are the major long-range projection neurons in BSTLD and CeL/C. However, SOM+ cells might not be the only cell types involved in long-range projections. Indeed, several neuropeptidic markers, including ENK, CRF, and neurotensin, have also been detected in brainstem-projecting neurons of CeL/C and BSTLD, but also of CeM and BSTLV (Gray and Magnuson 1987, 1992; Magableh and Lundy 2014; Moga and Gray 1985; Moga et al. 1989).

Comparative aspects of cell-type specific circuits in EAc

We disclosed the organization of the microcircuits in the EAc of mice, yet, it is important to address the potential existence of such microcircuits in other species, especially in rats. The rat amygdala has been the subject of

an abundant literature since the 1970s (~ 15,000 PubMed entries), including numerous systematic analyses of its morphofunctional features, such as cytoarchitecture, connectivity, and neurochemistry. By comparison, studies on the mouse amygdala became significant only since the 2000s (~ 4300 PubMed entries) and often focus on a specific functional topic, with a multiscale approach ranging from cellular aspects to behavior. The situation is similar for the BST, with much less publications (PubMed: ~ 2250 in rat and ~ 550 in mouse). As a consequence, the connectivity of the rat amygdala and BST has been widely described at mesoscopic scale (Cassell et al. 1999; Dong et al. 2001a, b; Jolkkonen and Pitkanen 1998; Krettek and Price 1978; McDonald et al. 1999; Sun et al. 1991), but, so far, the identification of cell-type specific microcircuits has been done mostly in mice (Cai et al. 2014; Ciocchi et al. 2010; Haubensak et al. 2010; Kim et al. 2017; Li et al. 2013). Yet, the notion of EAc as an anatomofunctional macrosystem, based on intimate interconnections between CeA and BSTL, is largely accepted in rats, mice, monkeys, and human (Alheid 2003; Fox et al. 2015; Martin et al. 1991; Oler et al. 2017; Shackman and Fox 2016; Zahm 2006). Considering the conservation of EAc in mammals, it is probably safe to assume than the general organization of extrinsic and intrinsic EAc circuits may follow the same basic rules, but with potential differences in specific actors. For example, Kaufling et al. (2017) showed a stronger projection from BSTL to the ventral tegmental area in mice than in rats. On the other hand, the outputs of BSTLD CRF+ neurons appear to be largely comparable in both rodent species (Dabrowska et al. 2016). Regarding the neuronal populations underlying the microcircuits described here, SOM+ cells have been shown to contribute to the BSTL and CeA outputs to brainstem targets in rats (Gray and Magnuson 1987, 1992; Moga and Gray 1985; Moga et al. 1989), consistent with our results in mice. The connections of PKCδ+ neurons in the rat EAc are, however, not described, and, while such neurons exist in the rat CeL, their physiological properties may be different than those in mice (Amano et al. 2012). Similarly, neurons in rat the BSTL have been classified in three physiological types (types I, II, and III), based on their electrophysiological properties (Hammack et al. 2007), but a recent comparative study showed that, even though the three types are also present in the BSTL of mice and monkeys, their proportions are different and some neuronal properties may also differ (Daniel et al. 2017). It is then possible than their physiological roles and their place in the circuits may also differ, as well as their cellular markers. Thus, the cell-type specific EAc microcircuits described in the mouse can provide a working frame to test their existence in other species.

Functional implications of cell-type specific circuits in EAc

The pioneer studies of Cassell's group (Cassell et al. 1999, 1986; Sun and Cassell 1993; Sun et al. 1991, 1994) established the notion that in the rat CeA, the CeL (and CeC) constitutes an inhibitory interface between extra-EAc inputs and the CeA outputs, derived from CeM. The organization of this microcircuitry was later refined in mice by showing that, in fear conditioning, a conditioned stimulus, previously associated with an unconditioned stimulus, activates in CeL/C a population of PKCδ− cells, potentially SOM+, which inhibits, in turn, a population of PKCδ+ cells projecting to CeM, leading, thus, to the disinhibition of the CeM outputs neurons (Ciocchi et al. 2010; Haubensak et al. 2010). Subsequent studies have detailed the roles of CeL/C PKCδ+ and SOM+ cells, along with LPB CGRP+ input, in fear learning and memory, in fear generalization and anxiety behaviors (Botta et al. 2015; Han et al. 2015; Li et al. 2013; Penzo et al. 2015). The role of these CeA circuits in feeding has also been examined through elegant studies, showing that LPB CGRP+ signaling to PKCδ+ CeL/C suppresses appetite, while other inputs, including those from BL, can target other cell populations (i.e. SOM+ and Htr2a+) that promote appetite (Cai et al. 2014; Campos et al. 2016; Carter et al. 2013; Douglass et al. 2017; Kim et al. 2017). The CeA circuit that we described here is consistent with the connectivity revealed in these studies. By contrast, this level of refinement in microcircuits has not yet been reached for BSTL. The BSTL has been shown to be largely involved in contextual fear learning, anxiety states, and stress response (Daldrup et al. 2016; Davis et al. 2010; De Bundel et al. 2016; Goode et al. 2015; Zimmerman and Maren 2011). De Bundel and colleagues showed that fear generalization relays on a coordinated action of D2R-expressing neurons in BSTLD and CeL/C, which mostly coexpress PKCδ (De Bundel et al. 2016). Thus, considering the parallel circuits existing in CeL/C and BSTLD, it is possible that LPB →BSTLD pathway uses a similar microcircuitry as LPB →CeL/C to support BSTL roles in associative learning and memory or in feeding.

Concluding remarks

Although the main components of EAc are well known to substantially share input/output connectivity and neurochemical features, comparative studies of BSTL and CeA neuronal circuits at cellular level are missing. In this study, we revealed a new depth of structural similarity between BSTLD and CeL/C in mice by showing the existence of similar cell-type specific neuronal circuits in both nuclei. We showed that, like in CeA, the non-overlapping PKCδ+

and SOM+ neuronal populations also exist in BSTL. In both nuclei, these two distinct neuronal groups form cell-type specific microcircuits integrating long-range inputs, mediating intrinsic connections, and sending long-range projections. In addition, these parallel microcircuits are, at the same time, integrated circuits, largely through interconnections within nuclei, between BSTLD and CeL/C and from BSTLD to CeM as well as from CeL/C to BSTLV.

Experiments carried out on BSTL and CeA as individual nuclei often led to the notion that they may be either agonistic or antagonistic pairs of nuclei. However, this interpretation may overshadow the fact that the EAc exerts a bidirectional regulation on emotional states and behaviors, through discrete microcircuits distributed across the subdivisions of BSTL and CeA. The two nuclei share similarly organized microcircuits, based on a cell-specific intra-nuclear connectivity (inside BSTL or CeA), but also on an inter-nuclear crosstalk (between BSTLD and CeL/C, from BSTLD to CeM, and from CeL/C to BSTLV). As these four subdivisions can provide direct projections to the hypothalamus and the brainstem, the integrated output of the EAc would rely on multiple channels, thus requiring a strong cooperation between its components. In addition, the essentially GABAergic nature of EAc intrinsic connections can generate apparent antagonism between BSTL and CeA through direct inhibition, but also agonism through disinhibitory mechanisms involving cell-specific microcircuits. For example, it has been shown that BSTL and CeA can both promote appetitive or avoidance behaviors, depending on the considered subdivisions and neurochemically defined neuronal populations (Giardino et al. 2018; Kim et al. 2017).

On the other hand, CeA and BSTL are known to be involved in negative emotions, but with distinct roles. For instance, it has been suggested that the BSTL is more involved in unconditioned/sustained response to threat (e.g., anxiety-like behavior), while the CeA is more implicated in conditioned/phasic response (e.g., fear) (Davis et al. 2010; Lebow and Chen 2016; Walker and Davis 1997; Walker et al. 2003). The current view, based on the hypothesis of Davis et al. (2010), proposes that the CeA triggers a rapid response to threat, through a CeL/C-to-CeM circuit, while more diffuse, but persistent, threats would engage a CeL/C to BSTL circuit, that mediates sustained responses and ultimately decreases phasic responses by BSTL to CeM inhibition (Shackman and Fox 2016). BSTL and CeA can exert positive or negative influences on emotional states. In the CeL/C, activation of PKCδ+ cells decreases anxiety-like behaviors in an elevated plus maze test (Cai et al. 2014). In the BSTL, Kim et al. (2013) showed that chemical or optogenetic stimulation of the whole BSTLD promotes anxious state features, while stimulation of BSTLP, a subdivision sharing functional features with BSTLV, has an anxiolytic influence. These specific effects can, however, rely on coordinated actions between EAc subdivisions. Indeed, optogenetic stimulation of CeA-projecting neurons in the rat BSTLD increased anxiety in an elevated plus maze test (Yamauchi et al. 2018) and Ahrens et al. (2018) demonstrated in mice that overactivation of SOM+ cells in the CeL/C promotes anxiety-like behaviors by disinhibiting BSTLD SOM+ cells. Thus, while several pieces of the puzzle are still missing, it appears that the necessary cooperation between CeA and BSTL to regulate anxiety is achieved through multiple inhibitory specific microcircuits, including those described here.

A similar organization could support the roles of EAc in pain. The CeA participates in both sensory and affective aspects of pain (Carrasquillo and Gereau 2007; Neugebauer 2015; Neugebauer et al. 2004; Veinante et al. 2013), while BSTL seems to contribute mainly to the affective component (Deyama et al. 2008; Minami and Ide 2015). It is, thus, possible that the affective component of pain is actually regulated by a coordinated activity of BSTL and CeA.

Thus, the similar, but distinct, BSTL and CeA act as an ensemble (EAc) to trigger and control responses to immediate and longer lasting environmental stimuli, including, but not restricted to, threats. The multiple cell-specific microcircuits inside and across BSTL and CeA would confer a large flexibility on EAc to adapt its responses in different situations. So far, it is not clear what kind of structural differences underlies the specificities of BSTL and CeA. One possibility could be the existence of subtle differences in the inputs and outputs circuits of BSTL and CeA, as well as in the specificity of local neuronal pools. For example, it remains to be explored whether BSTL and CeA are innervated by different sets of neurons in LPB or InsCx, or whether different pools of PKCδ+ or SOM+ neurons are involved in the specific aspects of fear/anxiety or sensory/affective components of pain. Another explanation could be the asymmetric connections between BSTLD and CeA, where the projection from CeA to BSTL is often reported to be stronger than that of the reverse direction (Dong et al. 2001a; Oler et al. 2017). Again, the functional implications of these structural differences remain to be further explored.

So far, compared to BSTL, the structures and functions of CeA microcircuits have been better studied by cell-type/pathway-specific genetic manipulation and behavioral assays (Cai et al. 2014; Ciocchi et al. 2010; Han et al. 2015; Haubensak et al. 2010; Li et al. 2013). Our results demonstrate that CeA-like microcircuits also exist in BSTL, and that they contribute to a complex network linking the components of the EAc. Future studies on structures and functions of neuronal circuits of BSTL might benefit from considering the previous studies of CeA microcircuits.

Acknowledgements This work was supported by the Centre National de la Recherche Scientifique (contract UPR3212), the University of

Strasbourg, and the NeuroTime Erasmus Mundus Joint Doctorate Program. We thank the Chronobiotron UMS3415 for animal housing and care, and the platform "in vivo imaging" at UPS3156. We thank Dr. Paul Klosen for the helpful advices in CARD method and Dr. Alessandro Bilella for the help in using NanoZoomer S60 platform.

Compliance with ethical standards

Conflict of interest The authors declare that they have no conflict of interest.

Ethical approval All applicable international, national, and/or institutional guidelines for the care and use of animals were followed.

Informed consent No human subject was used in this study.

References

Ahrens S et al (2018) A Central Extended Amygdala Circuit That Modulates. Anxiety J Neurosci 38:5567–5583

Alden M, Besson JM, Bernard JF (1994) Organization of the efferent projections from the pontine parabrachial area to the bed nucleus of the stria terminalis and neighboring regions: a PHA-L study in the rat. J Comp Neurol 341:289–314. https://doi.org/10.1002/cne.903410302

Alheid GF Ann (2003) Extended amygdala and basal forebrain. N Y Acad Sci 985:185–205. https://doi.org/10.1111/j.1749-6632.2003.tb07082.x

Amano T, Amir A, Goswami S, Pare D (2012) Morphology, PKCdelta expression, and synaptic responsiveness of different types of rat central lateral amygdala neurons. J Neurophysiol 108:3196–3205

Bernard JF, Alden M, Besson JM (1993) The organization of the efferent projections from the pontine parabrachial area to the amygdaloid complex: a Phaseolus vulgaris leucoagglutinin (PHA-L) study in the rat. J Comp Neurol 329:201–229. https://doi.org/10.1002/cne.903290205

Botta P et al (2015) Regulating anxiety with extrasynaptic inhibition. Nat Neurosci 18:1493–1500. https://doi.org/10.1038/nn.4102

Cai H, Haubensak W, Anthony TE, Anderson DJ (2014) Central amygdala PKC-delta(+) neurons mediate the influence of multiple anorexigenic signals. Nat Neurosci 17:1240–1248. https://doi.org/10.1038/nn.3767

Campos CA, Bowen AJ, Schwartz MW, Palmiter RD (2016) Parabrachial CGRP Neurons Control Meal. Termination Cell Metab 23:811–820. https://doi.org/10.1016/j.cmet.2016.04.006

Carrasquillo Y, Gereau RWt (2007) Activation of the extracellular signal-regulated kinase in the amygdala modulates pain perception. J Neurosci 27:1543–1551. https://doi.org/10.1523/JNEUROSCI.3536-06.2007

Carter ME, Soden ME, Zweifel LS, Palmiter RD (2013) Genetic identification of a neural circuit that Suppresses appetite. Nature 503:111–114. https://doi.org/10.1038/nature12596

Cassell MD, Gray TS, Kiss JZ (1986) Neuronal architecture in the rat central nucleus of the amygdala: a cytological, hodological, and immunocytochemical study. J Comp Neurol 246:478–499. https://doi.org/10.1002/cne.902460406

Cassell MD, Freedman LJ, Shi C (1999) The intrinsic organization of the central extended amygdala Ann. N Y Acad Sci 877:217–241

Ciocchi S et al (2010) Encoding of conditioned fear in central amygdala inhibitory. Circ Nat 468:277–282. https://doi.org/10.1038/nature09559

D'Hanis W, Linke R, Yilmazer-Hanke DM (2007) Topography of thalamic and parabrachial calcitonin gene-related peptide (CGRP) immunoreactive neurons projecting to subnuclei of the amygdala and extended amygdala. J Comp Neurol 505:268–291. https://doi.org/10.1002/ene.21495

Dabrowska J, Martinon D, Moaddab M, Rainnie DG (2016) Targeting corticotropin-releasing factor projections from the oval nucleus of the bed nucleus of the stria terminalis using cell-type specific neuronal tracing studies in mouse and rat Brain J Neuroendocrinol. https://doi.org/10.1111/jne.12442

Daldrup T, Lesting J, Meuth P, Seidenbecher T, Pape HC (2016) Neuronal correlates of sustained fear in the anterolateral part of the bed nucleus of stria terminalis. Neurobiol Learn Mem 131:137–146. https://doi.org/10.1016/j.nlm.2016.03.020

Daniel SE, Guo J, Rainnie DG (2017) A comparative analysis of the physiological properties of neurons in the anterolateral bed nucleus of the stria terminalis in the Mus musculus, Rattus norvegicus, and Macaca mulatta. J Comp Neurol 525:2235–2248. https://doi.org/10.1002/cne.24202

Davis M, Shi C (1999) The extended amygdala: are the central nucleus of the amygdala and the bed nucleus of the stria terminalis differentially involved in fear versus anxiety? Ann N Y Acad Sci 877:281–291

Davis M, Walker DL, Miles L, Grillon C (2010) Phasic vs sustained fear in rats and humans: role of the extended amygdala in fear vs anxiety. Neuropsychopharmacology 35:105–135. https://doi.org/10.1038/npp.2009.109

de Olmos JS, Heimer L (1999) The concepts of the ventral striatopallidal system and extended amygdala. Ann N Y Acad Sci 877:1–32

De Bundel D, Zussy C, Espallergues J, Gerfen CR, Girault JA, Valjent E (2016) Dopamine D2 receptors gate generalization of conditioned threat responses through mTORC1 signaling in the extended amygdala. Mol Psychiatry 21:1545–1553. https://doi.org/10.1038/mp.2015.210

Delaney AJ, Crane JW, Sah P (2007) Noradrenaline modulates transmission at a central synapse by a presynaptic mechanism. Neuron 56:880–892. https://doi.org/10.1016/j.neuron.2007.10.022

Deyama S et al (2008) Activation of the beta-adrenoceptor-protein kinase A signaling pathway within the ventral bed nucleus of the stria terminalis mediates the negative affective component of pain in rats. J Neurosci 28:7728–7736. https://doi.org/10.1523/JNEUROSCI.1480-08.2008

Dobolyi A, Irwin S, Makara G, Usdin TB, Palkovits M (2005) Calcitonin gene-related peptide-containing pathways in the rat forebrain. J Comp Neurol 489:92–119. https://doi.org/10.1002/cne.20618

Dong HW, Petrovich GD, Swanson LW (2001a) Topography of projections from amygdala to bed nuclei of the stria terminalis. Brain Res Brain Res Rev 38:192–246

Dong HW, Petrovich GD, Watts AG, Swanson LW (2001b) Basic organization of projections from the oval and fusiform nuclei of the bed nuclei of the stria terminalis in adult rat brain. J Comp Neurol 436:430–455

Douglass AM et al (2017) Central amygdala circuits modulate food consumption through a positive-valence mechanism. Nat Neurosci 20:1384–1394. https://doi.org/10.1038/nn.4623

Fadok JP et al (2017) A competitive inhibitory circuit for selection of active and passive fear responses. Nature 542:96–100. https://doi.org/10.1038/nature21047

Fox AS, Oler JA, Tromp do PM, Fudge JL, Kalin NH (2015) Extending the amygdala in theories of threat processing. Trends Neurosci 38:319–329 doi:S0166-2236(15)00061-2 [pii]

Franke-Radowiecka A (2011) Immunohistochemical characterisation of dorsal root ganglia neurons supplying the porcine mammary gland. Histol Histopathol 26(12):1509–1517. https://doi.org/10.14670/HH-26.1509

Giardino WJ, Eban-Rothschild A, Christoffel DJ, Li SB, Malenka RC, de Lecea L (2018) Parallel circuits from the bed nuclei of stria terminalis to the lateral hypothalamus drive opposing emotional states. Nat Neurosci 21:1084–1095. https://doi.org/10.1038/s41593-018-0198-x

Goode TD, Kim JJ, Maren S (2015) Reversible inactivation of the bed nucleus of the stria terminalis prevents reinstatement but not renewal of extinguished fear. eNeuro https://doi.org/10.1523/ENEURO.0037-15.2015

Gray TS, Magnuson DJ (1987) Neuropeptide neuronal efferents from the bed nucleus of the stria terminalis and central amygdaloid nucleus to the dorsal vagal complex in the rat. J Comp Neurol 262:365–374. https://doi.org/10.1002/cne.902620304

Gray TS, Magnuson DJ (1992) Peptide immunoreactive neurons in the amygdala and the bed nucleus of the stria terminalis project to the midbrain central gray in the rat. Peptides 13:451–460

Gungor NZ, Pare D (2016) Functional heterogeneity in the bed nucleus of the stria terminalis. J Neurosci 36:8038–8049. https://doi.org/10.1523/JNEUROSCI.0856-16.2016

Gungor NZ, Yamamoto R, Pare D (2015) Optogenetic study of the projections from the bed nucleus of the stria terminalis to the central amygdala. J Neurophysiol 114:2903–2911. https://doi.org/10.1152/jn.00677.2015

Hammack SE, Mania I, Rainnie DG (2007) Differential expression of intrinsic membrane currents in defined cell types of the anterolateral bed nucleus of the stria terminalis. J Neurophysiol 98:638–656

Han S, Soleiman MT, Soden ME, Zweifel LS, Palmiter RD (2015) Elucidating an affective pain circuit that creates a. Threat Memory Cell 162:363–374. https://doi.org/10.1016/j.cell.2015.05.057

Haubensak W et al (2010) Genetic dissection of an amygdala microcircuit that gates conditioned fear. Nature 468:270–276. https://doi.org/10.1038/nature09553

Higgins GA, Schwaber JS (1983) Somatostatinergic projections from the central nucleus of the amygdala to the vagal nuclei. Peptides 4:657–662

Hopkins DA, Holstege G (1978) Amygdaloid projections to the mesencephalon, pons and medulla oblongata in the cat. Exp Brain Res 32:529–547

Hunt S, Sun Y, Kucukdereli H, Klein R, Sah P (2017) Intrinsic circuits in the lateral central Amygdala. eNeuro. https://doi.org/10.1523/ENEURO.0367-16.2017

Hunyady B, Krempels K, Harta G, Mezey E (1996) Immunohistochemical signal amplification by catalyzed reporter deposition and its application in double immunostaining. J Histochem Cytochem 44:1353–1362

Janak PH, Tye KM (2015) From circuits to behaviour in the amygdala. Nature 517:284–292. https://doi.org/10.1038/nature14188

Jennings JH, Sparta DR, Stamatakis AM, Ung RL, Pleil KE, Kash TL, Stuber GD (2013) Distinct extended amygdala circuits for divergent motivational states. Nature 496:224–228. https://doi.org/10.1038/nature12041

Jhou TC, Geisler S, Marinelli M, Degarmo BA, Zahm DS (2009) The mesopontine rostromedial tegmental nucleus: a structure targeted by the lateral habenula that projects to the ventral tegmental area of Tsai and substantia nigra compacta. J Comp Neurol 513:566–596. https://doi.org/10.1002/cne.21891

Jolkkonen E, Pitkanen A (1998) Intrinsic connections of the rat amygdaloid complex: projections originating in the central nucleus. J Comp Neurol 395:53–72 https://doi.org/10.1002/(SICI)1096-9861(19980525)395:1%3C53

Kaufling J, Girard D, Maitre M, Leste-Lasserre T, Georges F (2017) Species-specific diversity in the anatomical and physiological organisation of the BNST-VTA pathway. Eur J Neurosci 45:1230–1240. https://doi.org/10.1111/ejn.13554

Kim SY et al (2013) Diverging neural pathways assemble a behavioural state from separable features in anxiety. Nature 496:219–223. https://doi.org/10.1038/nature12018

Kim J, Zhang X, Muralidhar S, LeBlanc SA, Tonegawa S (2017) Basolateral to central Amygdala neural circuits for appetitive behaviors. Neuron 93:1464–1479 e1465. https://doi.org/10.1016/j.neuron.2017.02.034

Koob GF (2003) Neuroadaptive mechanisms of addiction: studies on the extended amygdala. Eur Neuropsychopharmacol 13:442–452

Krettek JE, Price JL (1978) Amygdaloid projections to subcortical structures within the basal forebrain and brainstem in the rat and cat. J Comp Neurol 178:225–254. https://doi.org/10.1002/cne.901780204

Kudo T et al (2012) Three types of neurochemical projection from the bed nucleus of the stria terminalis to the ventral tegmental area in adult mice. J Neurosci 32:18035–18046

Larriva-Sahd J (2006) Histological and cytological study of the bed nuclei of the stria terminalis in adult rat. II. Oval nucleus: extrinsic inputs, cell types, neuropil, and neuronal modules. J Comp Neurol 497:772–807. https://doi.org/10.1002/cne.21011

Lebow MA, Chen A (2016) Overshadowed by the amygdala: the bed nucleus of the stria terminalis emerges as key to psychiatric disorders. Mol Psychiatry 21:450–463. https://doi.org/10.1038/mp.2016.1

Lein ES et al (2007) Genome-wide atlas of gene expression in the adult mouse brain. Nature 445:168–176. https://doi.org/10.1038/nature05453

Li H, Penzo MA, Taniguchi H, Kopec CD, Huang ZJ, Li B (2013) Experience-dependent modification of a central amygdala fear circuit. Nat Neurosci 16:332–339. https://doi.org/10.1038/nn.3322

Magableh A, Lundy R (2014) Somatostatin and corticotrophin releasing hormone cell types are a major source of descending input from the forebrain to the parabrachial nucleus in mice. Chem Senses 39:673–682. https://doi.org/10.1093/chemse/bju038

Martin LJ, Powers RE, Dellovade TL, Price DL (1991) The bed nucleus-amygdala continuum in human and monkey. J Comp Neurol 309:445–485

Mazzone CM et al (2016) Acute engagement of Gq-mediated signaling in the bed nucleus of the stria terminalis induces anxiety-like behavior. Mol Psychiatry. https://doi.org/10.1038/mp.2016.218

McDonald AJ (1991) Topographical organization of amygdaloid projections to the caudatoputamen, nucleus accumbens, and related striatal-like areas of the rat brain. Neuroscience 44:15–33

McDonald AJ, Shammah-Lagnado SJ, Shi C, Davis M (1999) Cortical afferents to the extended amygdala. Ann N Y Acad Sci 877:309–338

Minami M, Ide S (2015) How does pain induce negative emotion? Role of the bed nucleus of the stria terminalis in pain-induced place aversion. Curr Mol Med 15:184–190

Moga MM, Gray TS (1985) Evidence for corticotropin-releasing factor, neurotensin, and somatostatin in the neural pathway from the central nucleus of the amygdala to the parabrachial nucleus. J Comp Neurol 241:275–284. https://doi.org/10.1002/cne.902410304

Moga MM, Saper CB, Gray TS (1989) Bed nucleus of the stria terminalis: cytoarchitecture, immunohistochemistry, and projection to the parabrachial nucleus in the rat. J Comp Neurol 283:315–332. https://doi.org/10.1002/cne.902830302

Neugebauer V (2015) Amygdala pain mechanisms Handb. Exp Pharmacol 227:261–284. https://doi.org/10.1007/978-3-662-46450-2_13

Neugebauer V, Li W, Bird GC, Han JS (2004) The amygdala persistent pain. Neuroscientist 10:221–234. https://doi.org/10.1177/1073858403261077

Nguyen AQ, Dela Cruz JA, Sun Y, Holmes TC, Xu X (2016) Genetic cell targeting uncovers specific neuronal types and distinct subregions in the bed nucleus of the stria terminalis. J Comp Neurol. https://doi.org/10.1002/cne.23954

Oh SW et al (2014) A mesoscale connectome of the mouse brain. Nature 508:207–214. https://doi.org/10.1038/nature13186

Oler JA et al (2017) Connectivity between the central nucleus of the amygdala and the bed nucleus of the stria terminalis in the non-human primate: neuronal tract tracing and developmental neuroimaging studies. Brain Struct Funct 222:21–39. https://doi.org/10.1007/s00429-016-1198-9

Panguluri S, Saggu S, Lundy R (2009) Comparison of somatostatin and corticotrophin-releasing hormone immunoreactivity in forebrain neurons projecting to taste-responsive and non-responsive regions of the parabrachial nucleus in rat. Brain Res 1298:57–69. https://doi.org/10.1016/j.brainres.2009.08.038

Paxinos G, Franklin K (2012) Paxinos and Franklin's the mouse brain in stereotaxic coordinates. Academic Press, Amsterdam

Penzo MA, Robert V, Li B (2014) Fear conditioning potentiates synaptic transmission onto long-range projection neurons in the lateral subdivision of central amygdala. J Neurosci 34:2432–2437. https://doi.org/10.1523/JNEUROSCI.4166-13.2014

Penzo MA et al (2015) The paraventricular thalamus controls a central amygdala fear circuit. Nature https://doi.org/10.1038/nature13978

Petrovich GD, Swanson LW (1997) Projections from the lateral part of the central amygdalar nucleus to the postulated fear conditioning circuit. Brain Res 763:247–254

Pitkanen A, Stefanacci L, Farb CR, Go GG, LeDoux JE, Amaral DG (1995) Intrinsic connections of the rat amygdaloid complex: projections originating in the lateral nucleus. J Comp Neurol 356:288–310. https://doi.org/10.1002/cne.903560211

Pitkanen A, Savander M, Nurminen N, Ylinen A (2003) Intrinsic synaptic circuitry of the amygdala Ann. N Y Acad Sci 985:34–49

Pomrenze MB et al (2015) A transgenic rat for investigating the anatomy and function of corticotrophin releasing factor. Circ Front Neurosci 9:487. https://doi.org/10.3389/fnins.2015.00487

Salio C, Averill S, Priestley JV, Merighi A (2007) Costorage of BDNF and neuropeptides within individual dense-core vesicles in central and peripheral neurons. Dev Neurobiol 67:326–338. https://doi.org/10.1002/dneu.20358

Saper CB (1982) Convergence of autonomic and limbic connections in the insular cortex of the rat. J Comp Neurol 210:163–173. https://doi.org/10.1002/cne.902100207

Sarhan M, Freund-Mercier MJ, Veinante P (2005) Branching patterns of parabrachial neurons projecting to the central extended amygdala: single axonal reconstructions. J Comp Neurol 491:418–442. https://doi.org/10.1002/cne.20697

Sato M, Ito M, Nagase M, Sugimura YK, Takahashi Y, Watabe AM, Kato F (2015) The lateral parabrachial nucleus is actively involved in the acquisition of fear memory in mice. Mol Brain 8:22. https://doi.org/10.1186/s13041-015-0108-z

Savander V, Go CG, Ledoux JE, Pitkanen A (1996) Intrinsic connections of the rat amygdaloid complex: projections originating in the accessory basal nucleus. J Comp Neurol 374:291–313

Schindelin J et al (2012) Fiji: an open-source platform for biological-image analysis. Nat Methods 9:676–682. https://doi.org/10.1038/nmeth.2019

Shackman AJ, Fox AS (2016) Contributions of the central extended amygdala to fear and. Anxiety J Neurosci 36:8050–8063. https://doi.org/10.1523/JNEUROSCI.0982-16.2016

Speel EJ, Ramaekers FC, Hopman AH (1997) Sensitive multicolor fluorescence in situ hybridization using catalyzed reporter deposition (CARD) amplification. J Histochem Cytochem 45:1439–1446

Sun N, Cassell MD (1993) Intrinsic GABAergic neurons in the rat central extended amygdala. J Comp Neurol 330:381–404. https://doi.org/10.1002/cne.903300308

Sun N, Roberts L, Cassell MD (1991) Rat central amygdaloid nucleus projections to the bed nucleus of the stria terminalis. Brain Res Bull 27:651–662

Sun N, Yi H, Cassell MD (1994) Evidence for a GABAergic interface between cortical afferents and brainstem projection neurons in the rat central extended amygdala. J Comp Neurol 340:43–64. https://doi.org/10.1002/cne.903400105

Thompson RH, Swanson LW (2010) Hypothesis-driven structural connectivity analysis supports network over hierarchical model of brain architecture. Proc Natl Acad Sci USA 107(34):15235–15239. https://doi.org/10.1073/pnas.1009112107

Tokita K, Inoue T, Boughter JD (2009) Afferent connections of the parabrachial nucleus in C57BL/6. J Mice Neurosci 161:475–488. https://doi.org/10.1016/j.neuroscience.2009.03.046

Veening JG, Swanson LW, Sawchenko PE (1984) The organization of projections from the central nucleus of the amygdala to brainstem sites involved in central autonomic regulation: a combined retrograde transport-immunohistochemical study. Brain Res 303:337–357

Veinante P, Freund-Mercier MJ (1998) Intrinsic and extrinsic connections of the rat central extended amygdala: an in vivo electrophysiological study of the central amygdaloid nucleus. Brain Res 794:188–198

Veinante P, Freund-Mercier MJ (2003) Branching patterns of central amygdaloid nucleus efferents in the rat: single-axon reconstructions. Ann N Y Acad Sci 985:552–553. https://doi.org/10.1111/j.1749-6632.2003.tb07126.x

Veinante P, Stoeckel ME, Freund-Mercier MJ (1997) GABA- and peptide-immunoreactivities co-localize in the rat central extended amygdala. Neuroreport 8:2985–2989

Veinante P, Yalcin I, Barrot M (2013) The amygdala between sensation and affect: a role in pain. J Mol Psychiatry 1:9. https://doi.org/10.1186/2049-9256-1-9

Walker DL, Davis M (1997) Double dissociation between the involvement of the bed nucleus of the stria terminalis and the central nucleus of the amygdala in startle increases produced by conditioned versus unconditioned fear. J Neurosci 17:9375–9383

Walker DL, Toufexis DJ, Davis M (2003) Role of the bed nucleus of the stria terminalis versus the amygdala in fear, stress, and anxiety. Eur J Pharmacol 463:199–216

Waraczynski M (2016) Toward a systems-oriented approach to the role of the extended amygdala in adaptive responding. Neurosci Biobehav Rev 68:177–194

Weller KL, Smith DA (1982) Afferent connections to the bed nucleus of the stria terminalis. Brain Res 232:255–270

Wood J, Verma D, Lach G, Bonaventure P, Herzog H, Sperk G, Tasan RO (2016) Structure and function of the amygdaloid NPY system: NPY Y2 receptors regulate excitatory and inhibitory synaptic transmission in the centromedial amygdala. Brain Struct Funct 221:3373–3391. https://doi.org/10.1007/s00429-015-1107-7

Yamauchi N, Takahashi D, Sugimura YK, Kato F, Amano T, Minami M (2018) Activation of the neural pathway from the dorsolateral bed nucleus of the stria terminalis to the central amygdala induces anxiety-like behaviors. Eur J Neurosci 48:3052–3061. https://doi.org/10.1111/ejn.14165

Yasui Y, Breder CD, Saper CB, Cechetto DF (1991a) Autonomic responses and efferent pathways from the insular cortex in the rat. J Comp Neurol 303:355–374. https://doi.org/10.1002/cne.903030303

Yasui Y, Saper CB, Cechetto DF (1991b) Calcitonin gene-related peptide (CGRP) immunoreactive projections from the thalamus to the striatum and amygdala in the rat. J Comp Neurol 308:293–310. https://doi.org/10.1002/cne.903080212

Yu K, Garcia da Silva P, Albeanu DF, Li B (2016) Central amygdala somatostatin neurons gate passive and active defensive. Behaviors J Neurosci 36:6488–6496. https://doi.org/10.1523/JNEUROSCI.4419-15.2016

Zahm DS (2006) The evolving theory of basal forebrain functional-anatomical 'macrosystems'. Neurosci Biobehav Rev 30:148–172

Zimmerman JM, Maren S (2011) The bed nucleus of the stria terminalis is required for the expression of contextual but not auditory freezing in rats with basolateral amygdala lesions. Neurobiol Learn Mem 95:199–205. https://doi.org/10.1016/j.nlm.2010.11.002